1-1-2012

Mechanical And Structural Properties Of Ultra High Performance Fiber Reinforced Concrete

Kirllos Wahba
Ryerson University

MECHANICAL AND STRUCTURAL PROPERTIES OF ULTRA HIGH PERFORMANCE FIBER REINFORCED CONCRETE

by

Kirllos Wahba, B.Eng, Toronto, September 2012

A thesis

presented to Ryerson University

in partial fulfillment of the

requirements for the degree of

Master of Applied Science

in the Program of

Civil Engineering

Toronto, Ontario, Canada, 2012

AUTHOR'S DECLARATION

I hereby declare that I am the sole author of this thesis. This is a true copy of the thesis, including any required final revisions, as accepted by my examiners.

I authorize Ryerson University to lend this thesis to other institutions or individuals for the purpose of scholarly research

I further authorize Ryerson University to reproduce this thesis by photocopying or by other means, in total or in part, at the request of other institutions or individuals for the purpose of scholarly research.

I understand that my thesis may be made electronically available to the public.

Author signature__________________ Date__________________

MECHANICAL AND STRUCTURAL PROPERTIES OF ULTRA HIGH PERFORMANCE FIBER REINFORCED CONCRETE

Kirllos Wahba

Master of Applied Science, Civil Engineering

Ryerson University, Toronto, Canada, 2012

Abstract

Ultra High Performance Fiber Reinforced Concrete (UHPFRC) is beginning to revolutionize the construction industry. The research presented discusses an experimental program designed to investigate the mechanical and structural properties of UHPFRC. The mechanical properties focused on examining the tensile behavior by testing the fracture energy, tension stiffening and shear friction properties of UHPFRC. The structural properties focused on investigating behaviors such as; flexure and shear. The tensile behavior proved to be significantly improved by the use of fibers. Results show an ultimate tensile strength twice the cracking tensile strength. The shear friction was also enhanced due to the fiber reinforcement. Improved design equation, with great accuracy when compared to experimental results are proposed. The addition of fibers, significantly improved the shear and flexure behavior of reinforced beams. The influence of the fiber reinforcement was of very significant; promoting flexural failure in reinforced beams rather than the shear failure when compared to normal and high strength concrete.

Acknowledgements

This research project was funded by the National Science and Engineering Research Council of Canada and supported by Lafarge North America. Their financial support and collaboration is greatly appreciated.

I wish to express my deepest gratitude to my supervisor Dr. H. Marzouk, for providing me with the opportunity to pursue my graduate work. I would like to thank him for his continues support and guidance throughout the duration of this project. The concern he has for his students should be a model all his peers. It was truly a pleasure working under his supervision

None of my success would be possible without the help of Dr. N. Dawood throughout my research. I am truly thankful for the help of my peers Mr. D. Hughi and Mr. A. Sucic; their contribution is greatly appreciated. Also I would like to extend my gratitude to the technical staff of the Civil Engineering labs at Ryerson University. The support of Dr. M. Shehata is greatly valued. I would like to thank Dr. M. Shehata for encouraging me to pursue my graduate work after completion of my B. Eng degree.

Lastly I would like to thank my family and friends for their continues encouragement and support throughout my academic career

Table of Contents

List of Tables

List of Figures

DEDICATED TO MY FAMILY AND FRIENDS

Chapter [1]

Introduction

[1.1] General

While reinforced concrete can carry high stresses under compression, it proved to crack easily under tensile stresses. The development of cracks does not only affect the aesthetics of the structures but also exposes the steel reinforcement. Concrete cracks are developed under tensile stresses and such cracks have a significant effect on the reduction of the carrying capacity of the concrete section. In general practice, steel reinforcement bars are used to restrain crack opening and carry stresses across cracks once the tensile carrying capacity of the concrete is exceeded. Losses of bearing capacity and increase in permeability are some of the effects attributed to concrete cracking. Moreover, concrete with compressive strength greater than 50 MPa proved to behave in a very brittle manner. The addition of fibers to concrete to reduce the brittleness dates back to the 1980's. The fibers have additional positive effects on the concrete such as; increased compressive and tensile strength and enhanced post-cracking characteristics. Over the years there has been substantial development in the field of fiber reinforced concrete.

Ultra High Performance Fiber Reinforced Concrete (UHPFRC) is the current product of years of research in concrete development. UHPFRC is a class of materials that exhibits superior qualities to those of conventional concrete. UHPFRC is characterized by a relatively high elastic limit, strain hardening, and toughness associated with the multiple cracking mechanisms (Soranakom & Mobasher, 2007). These enhanced properties are achieved by integrating a fiber matrix with a precisely optimized blend of nano materials. There has been a growing use of UHPFRC around the world (Rebentrost, 2008; Resplendino, 2004). Previous research on structural behaviour has shown that UHPFRC beams experienced flexural failure with compared to concrete beams made with the same properties excluding fiber reinforcement (Bunje & Fehling, 2004). In addition, the interaction of the fiber reinforcement and the UHPC matrix allows small width, closely spaced cracks to occur and allows concrete to carry tensile stresses after cracking (Graybeal, 2008).

[1.2] Research Objective

The behaviour of a reinforced concrete member depends on the transfer of forces, via bond action, between the concrete and the reinforcement bars. When cracks are initiated the stresses are transferred across the crack by the reinforceing bar. The objective of this research is to inveestegate the effect of fiber reinforcement on the material and structural properties of concrete. The research at hand focuses specifically on UHPFRC.

Over the years UHPFRC has been subjected to numerous research and field trials. In today's growing construction industary, UHPFRC is used in a varaity of application that include but not limited to bridge girders and decks, joint fill construction, marine structures, pipe lines, piles, wall panels/facades, urban furniture, and stairs. Considred one of the leading materials specificly in bridge construction, UPPFRC's use is limited by the lack of design codes in North America. As the need for such materials increases; adequate design criteria is essential. The reserach at hand investegates the mechanical properties and structural behaviour of UHPFRC. The mechanical behaviour investegated included fracture energy, tension stiffening and shear friction. While the structural aspecy focuses on the flexural and shear behaviour. The study focuses of select prameters that have the most infulence on said behaviours.

[1.3] Thesis Overview

Chapter 2 reviews the previous development in concrete technology leading to UHPFRC. In addition a review of the earlier investigations conducted on concrete behaviour focusing on fiber reinforcement. A review of earlier equations proposed by researchers and design codes is summarized.

Chapter 3 outlines the experimental investigation conducted, as part of this research, to investigate the behaviour of UHPFRC. This research focused on investigating the mechanical properties of UHPFRC such as; fracture energy, tension stiffening and shear friction. Concrete beams were tested to investigate flexural capacity and shear behaviour.

Chapter 4 deals with the test results and analysis of the mechanical properties of UHPFRC. The results of the fracture energy is disscussed in details. The results of tension stiffening are also analyzed by investegating key prameters which affect the behaviour of the materials. In addition the shear friction results are analayzed and a simple design equation s proposed. Furthermore, the analysis of the shear friction behaviour is presented. The material properties of UHPFRC are compared to existing data found in the litreture review.

Chapter 5 disscusses the structural behaviour of UHPFRC. The results and the analysis UHPFRC beams under four point testing. Both flexure and shear behaviour is investegated by varing key prameters such; as reinforcement ration, shear reinforcement and shear span to depth ratio. The results are compared to pervious research to determine the adequacey of fiber reinforcement. Finally simple design equations are proposed to predict the flexural and the shear friction capacity of UHPFRC.

Laslty, chapter 6 sumarizes the findings of the research presented and outlines future reseach recommendation.

Chapter [2]

Literature Review

[2.1] Introduction

Since the 1950s the use of 35 MPa was considered to be high strength concrete (HSC), in today's industry concrete with compressive strength of almost 100 MPa has been used (ACI Committee 363 R, 2010). Ultra-High performance concrete (UHPC) is the current state of the art in concrete construction. UHPC is highly efficient due to its high compressive strength and performance. When fiber reinforcement is added to reduce the brittleness and increase energy absorption capacity the term Ultra High performance fibre reinforced concrete (UHPFRC) is used. UHPFRC is a class of materials that exhibits properties superior to those of conventional concrete. The superiority may lie in one or more of several attributes, such as freeze-thaw durability, scaling resistance, abrasion resistance, chloride penetration, and compressive strength, modulus of elasticity, shrinkage and creep. UHPFRC is a result of ongoing research and invention dated back to at least 30 years ago. UHPFRC is widely used all over the world and is not limited to North America. A versatile material, UHPFRC possesses desirable properties including strength, ductility, durability and aesthetic design flexibility. UHPFRC is specified where reduced weight is important or where architectural considerations require small load carrying members. Ongoing research in the field has pushed the limits of UHPFRC to greater levels. Laboratory research produced UHPFRC with compressive strength in excess of 800 MPa (ACI Committee 363 R, 2010; Wille & Naaman, 2011).

[2.2] Material Development

Since the appearance of effective dispersants for cement systems around the 1970s, many researchers have attempted to produce concrete with record compressive strength. Techniques such as vacuum mixing and hot temperatures and pressure were used to achieve such strength. Youdenfreund et at. (1972) achieved compressive strength of 230 MPa using vacuum mixing. Hot temperatures and pressure were introduced by Roy et al. (1972), obtaining compressive strength in the excess of 500 MPa. Later research, achieved compressive strength in the excess of 800 MPa by the introduction of high reactive powder concrete and steel fibers while using high pressure mixing and high temperature curing (Richard and Cheyrezy, 1995). However, using such techniques, pressure mixing and high temperature curing proved to be rather unpractical in the construction field.

Rather than the previous methodologies for mixing and curing, today's UHPFRC is produced with a precisely optimized blend of nano materials such as: silica fumes, quarts flour and silica sand. Its production however, is achieved by optimizing the following; characteristics of the cementing medium, characteristics of the aggregates, proportions of the paste, paste aggregate interaction, mixing, consolidating and curing. Wille and Naaman (2011) tested spread values according to ASTM C 230/C 230M standard and showed that increasing the silica fumes replacement from 0% to 25% significantly increased the spread values while achieving compressive strength up to 158 MPa. Such observation further proves the increase in packing degree when using silica fumes as a replacement for cement. In addition they tested glass powder replacement values and concluded that a replacement value of 20-30 % of cement resulted in compressive strength of 240 MPa

Furthermore Wille and Naaman (2011) investigated the effect of fiber geometry on concrete. They concluded that the use of twisted fibers or hooked end fibers increases the tensile strength as well as the tensile strain at peak stress when compared to smooth fibers. In addition increasing the fiber content within a certain range increases the tensile strength.

[2.2.1] Cement

A fundamental factor involved in producing UHPC is the cement paste. Without high grade cement the production of UHPC would not be possible. Control of cement fineness is a significant factor that affects the quality of the cement in use. Cement that yields to higher compressive strength at the latter stage, 90 days, is preferred. Lowering the sand content is the preferred method for increasing the cement content, as it allows for unchanged content of other ingredients.

[2.2.2] Fibers

Due to the nature of the material, concrete is extremely brittle showing a sudden loss of carrying capacity after the maximum load is exceeded. The addition of fibres, improved the post fracture nature of the material. The post fracture behavior is governed by the type and amount of fibres introduced in the mix. Use of longer fibres, 17 mm instead of 9 mm, reduced the amount of fibres required to achieve similar properties (Emplemann, 2008). Wille and Naaman (2011) proposed a limit of $l_f/d_f \times V_f = 2$ to the fiber content to preserve a suitable workability, where l_f is the fiber length, d_f is the fiber diameter and V_f is the fiber content

[2.2.3] Coarse Aggregate

Since coarse aggregate makes up most of the volume of concrete, its characteristics significantly influence the properties of concrete. In conventional concrete (35 MPa) the compressive strength is affected by the paste strength; since almost always the aggregate is stronger than the paste. However, in UHPFRC the strength of the paste surpasses the strength of the aggregate. In normal concrete the greater the maximum size of concrete the less water content is required. However, in UHPFRC the large aggregate tends to reduce the strength of the concrete probably because of the smaller surface area available for bond. However, in today's industry UHPFRC is produced without the addition of any coarse aggregate.

[2.2.4] Fine Aggregate

The shape and surface texture of fine aggregate have a significant effect on the water content, because of the larger surface area associated with fine aggregate. The cement bond to fine aggregate is less significant than that of course aggregate. Since all aggregate particles must be coated by cement, maximizing the ratio of course aggregate to fine aggregate is significant in UHPC. Rounded and smooth fine aggregates and natural sand produce stronger concrete. Concrete mixes of the same cement content and slump achieve greater compressive strength when compared to different types of fine aggregates. To date, UHPFRC has been produced with maximum particle size ranging from 800-200 μm (Wille and Naaman, 2011).

[2.2.5] Mixing Water

The use of water at 21º C, will increase the slump about 25-50 mm, which is desirable in terms of workability. If the amount of mixing water is consequently reduced, to compensate for the slump increase, the strength of the concrete will increase. However the use of cooler water is rarely available and the problems associated with the use of ice overtake the benefit of the small increase of strength.

[2.2.6] High Range Water Reducer

Super plasticisers in UHPC always exceed the manufacture recommended dosage for conventional concrete. Wille and Naaman (2011) investigated the effect of seven different SPLs on the production of UHPFRC. They concluded, while most SPLs are designed for a better cement dispersion, the most effective SPL should interact with all the fine particles for an overall enhanced dispersion.

[2.2.7] Mineral Admixtures

The mineral admixtures, also known as supplementary cementing materials (SCM), are of high significance to UHFRPC. SCMs are by-products materials that are added to concrete mixes to change some of the plastic or hardened properties of concrete. The two most commonly used

SCM in UHPFRC are fly ash and silica fumes. Silica fumes have played an important role in UHPC since it enhances the strength of concrete.

[2.3] Material Properties of Fiber Concrete

The addition of steel fibres to increase the compressive strength dates back to the 1980s (Sharma, 1986; Naraynan and Darwish, 1987). In the 1990s steel fibres were added to high strength concrete to reduce its brittleness behavior (Ashour et al., 1992). The increased ductility and post cracking tensile behavior resulted in increased tensile strength of high strength concrete made with fibre reinforcement (Kwak et al., 2002). UHPFRC is the current state of the art advancement in concrete technology (Lafarge North America, 2011). The incresed strength and perfoemence is a result of percies blending of Nano materials with steel fibres rather than high or normal fibre reinforced concrete made with conventional materials.

[2.3.1] Fracture Energy of Concrete

[2.3.1.1] Background

Numerous researches have been conducted to determine the structural behavior of concrete. Many authors suggest that the fracture characteristics of concrete are of upmost importance. Consequently, the fracture energy, G_f, tensile strength, f_t and the stress-crack mouth opening displacement (CMOD) relationship which completely describes the fracture characteristics of concrete (Hillerborg et al. 1976). Tensile strength of concrete is an essential property, though it is not directly used in design calculations. Nevertheless, not only is the tensile strength is important, the tensile fracture behavior is of significance. One way of quantifying fractural behavior of concrete is by means of fracture energy. Research has concluded that fracture energy tends to increases with an increase of maximum aggregate size from 8 to 20 mm (Rao and Prasad, 2002). However, other researches state the fracture energy increases with an increase in aggregate size and stiffness (Zhou F. , 1995). According to literature the method proposed, work-of-fracture, yield size dependent characteristics (Einsfeld and Velasco, 2006).

Consequently, the method yields different values for the fracture energy. Another proposed method, size effect method, yields values for fracture energy, which are independent of the size effect (Einsfeld and Velasco, 2006). Fracture energy; proved to be as significant, in designing for shear strength in beams and slabs, as traditional concrete properties.

[2.3.1.2] Direct Tension Method

The fracture energy, G_f, is defined as the area under the stress-deformation curve to form a unit area of crack surface (Petersson, 1980) represented by Eq. [2-1]; for specimens tested under direct tension. Where f_t is a function of tensile displacement δ_t and δ_{max} is the maximum tensile effective displacement when f_t reaches zero. It is recommended, unlike other materials, that energy absorbed by concrete members in tension is associated with the descending portion of the stress-displacement curve shown in Figure 2-1 (Hillerborg et al. 1976).

$$G_F = \int_0^{\delta_{max}} f_t d\delta_t \qquad \text{[Eq. 2-1]}$$

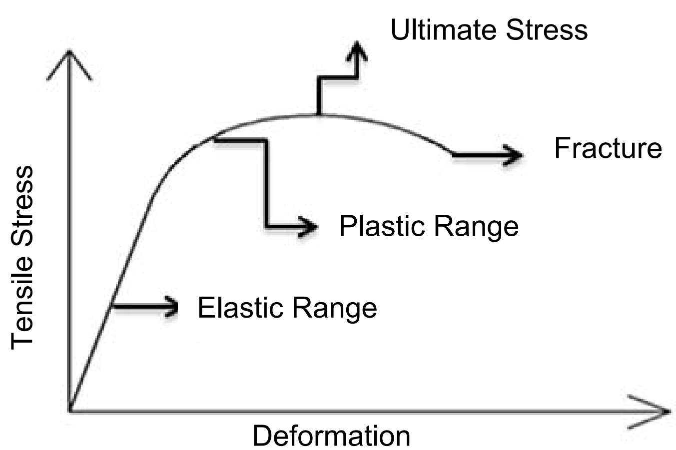

Figure 2-1 Stress-Strain Relation of Concrete

As the deformation is increased the stress initially increases, until reaching maximum stress, then decreases with the increase in the deformation. The descending portion of Figure 2-1 is referred to as strain softening (Hillerborg A. , 1985). This softening behavior takes place with a very small zone in the specimen, the fracture process zone. Subsequent to the development of the fracture zone, the strain is no longer evenly distributed along the specimen. The deformation increases within the damage zone, while decreasing within the rest of the specimen. The area under the graph represents the total amount of energy absorbed in a tensile test. The energy can be further divided into two phases: the area under the ascending curve represent the energy per unit volume, the area under the descending potion represents the energy absorbed within the fracture zone as shown in Figure 2-2 (Hillerborg A. , 1985).

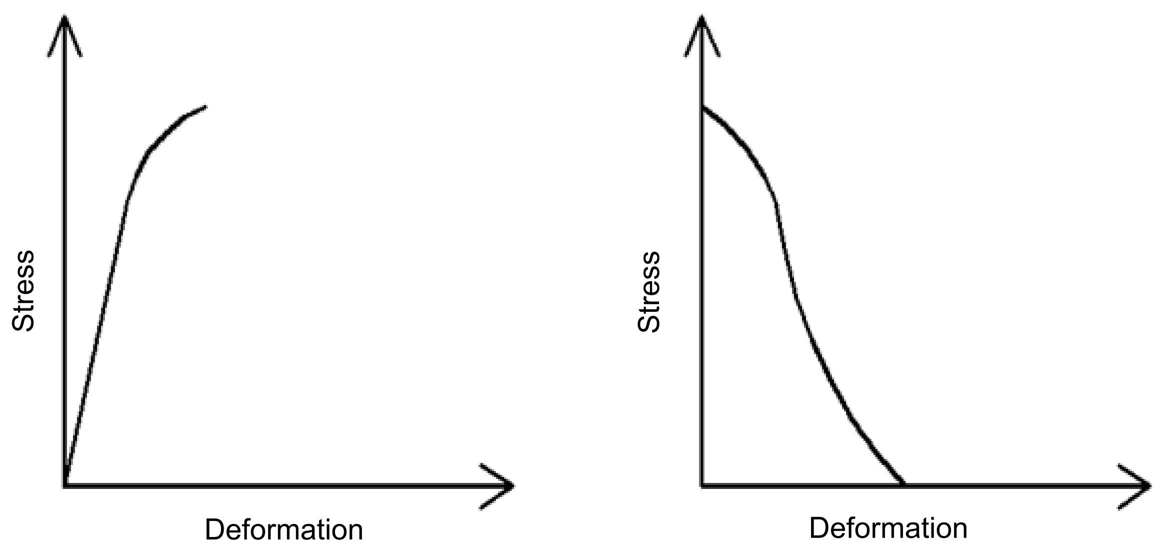

Figure 2-2 Description of tensile behavior by means of two curves, one curve for the whole volume (ascending) and one curve for additional deformation within the damage zone (descending) (Hillerborg, 1985)

Chen and Marzouk (1995) conducted a study on the behaviour of high strength concrete under pure tension. As a result of fracture energy testing, they concluded that high stregnth concrete has a more brittle failure when compared to normal strength concrete. Also, observed a sharp decending stress-strain curve after peak stress is reached. The brittleness behavior of concrete, made it almost impossible to capture the fracture energy of concrete due to the sudden failure under tensile stresses. However, when using UHPFRC it is expected, due to the fibre matrix, that an inelastic strain-hardening region could be captured. The region between the end of linear elastic range and the peak load denoted in Figure 2-3 is a result of multiple micro cracking. The linear elastic region, region I, represents the micro cracking stage. The softening stage, region III, corresponds to the single failure crack opening and is mainly controlled by the fibre pulling-out process (Martin and Stanton, 2007). Also the presence of fibre should eliminate the sudden fracture of the member, thus easing the fracture energy capturing.

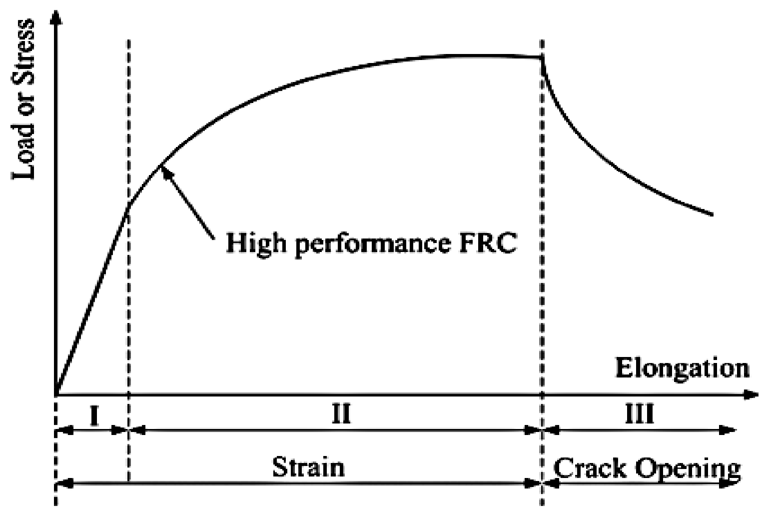

Figure 2-3 Stress-Strain Relations for Ultra High Performance Fibre reinforced Concrete (Martin & Stanton, 2007)

[2.3.1.3] Work of Fracture Method

While, direct tensile test yields the most accurate results, difficulties arise in terms of testing procedure. The most practical method for determination of fracture energy is by means of three or four point loading (Work-of-Fracture) (Petersson, 1980). The proposed method follows the same theoretical understanding of crack formation in concrete, thus making it the more preferred among researchers. The fracture energy can then be claculated according to the load-deformation response using Eq. [2-2] (Japan Concrete Institute Standard, 2003).

$G_F = (0.75W_0 + W_1)/A_{lig}$ [Eq. 2-2]

Where,

G_F = fracture energy (N/mm), W_1= 0.75(Sm_1/L +$2m_2$)*g*$CMOD_c$, W_0 = area below CMOD curve up to rupture of specimen (N.mm), W_1 = work done by deadweight of specimen and loading jig (N.mm), A_{lig} = area of broken ligament, m_1 = mass of specimen (kg). S = loading span (mm), L = total length of specimen (mm), m_2 = mass of jig not attached to testing machine but placed on specimen until rupture (kg), g = gravitational acceleration (9.807 m/s^2), $CMOD_c$ = crack mouth opening displacement at the time of rupture (mm)

Previous it was concluded that the fracture energy increases with the increase of compressive strength. Rao et al. (2002) reported fracture energy values ranging from 67-165 N/mm for concrete ranging in compressive strength ranging from 40-74 MPa respectively. Results obtained from experiments conducted by Einsfeld et al. (2006) can be compared with some results obtained by Rao et al. (2002) for specimens with the same size and notch depth. The results seem to follow the same trend of higher fracture energy for higher values of the compressive strength. A mean value for fracture energy of 120 N/m corresponding to a mean compressive strength of 48.5 MPa, seems to correspond with the results obtained from Rao et al. (2001).

[2.3.2] Tension Stiffening

It is well known that concrete continues to carry tensile stresses beyond cracking due to the bond between the reinforcement bars and the still intact concrete sections. This phenomenon, tension stiffening, was neglected in the past as it did not significantly increase the ultimate strength of reinforced concrete. Since the 70’s, however, the tensile behavior of concrete was introduced in the analysis of load-deflection characteristics of reinforced concrete elements, and since the 80s in design code recommendations for service load level. It is also important to consider tension-stiffening when evaluating the serviceability of existing reinforced concrete structures (Stramandinolie and Rovere, 2008). The tension-stiffening effect depends on several factors, such as member dimensions, reinforcement ratio, rebar's diameters, and the materials elastic modulus and strength. This effect occurs until yielding of the longitudinal reinforcement takes place, and it tends to increase as the reinforcement ratio of the member decreases.

Although concrete members subjected to pure tension do not often occur in practice, it became evident the examination of such case leads to fundamental understanding of the tension stiffening response. For a specified member elongation the reinforced concrete member requires a higher stress highlighting the tension stiffening response. As the load is increased beyond cracking the tension in the concrete reduces. It is the tension in the concrete which stiffens the response of the member. After cracking, the tension carried by the concrete is calculated as the net area of concrete times the average tensile stress in the concrete between the cracks.

Figure 2-4 shows a typical load-deformation response for a symmetrically reinforced axial member loaded in tension, where tension stiffening represents the difference between the member response and the bare steel bar response. The composite member response is initially linear elastic with uniform stresses in the concrete and steel along the length of the member, until the tensile strength of the concrete $f_t^{'}$ is reached and the member cracks at a load N_r. Once cracked, the concrete is not assumed to carry any tension at the cracks but it is still able to develop tensile stresses away from the crack as load is transferred from the reinforcing steel back into the surrounding concrete. Hence, stresses in the concrete vary between cracks along the length of the member, and this reduces the average tensile stress in the concrete as indicated in Figure 2-4 (Stevens et al., 1991).

In the past, numerous tension stiffening models were developed for normal strength and high strength concrete. However, since the introduction of fibres as means of reinforcement, fewer models exist. Since the fibers, carry stresses across cracks, via bridging action, it is evident that response of fibre reinforced concrete changes. Abrishami and Mitchell (1997) developed a simple model for tension stiffening of normal and high strength, 38 and 76 MPa respectively, fibre reinforced concrete, Eq. [2-8].

$$Nf = \frac{1}{6} V_f E_f A_c (\varepsilon - \varepsilon_y) \geq \frac{1}{6} V_f E_f f_{yf} \qquad \text{[Eq. 2-8]}$$

Where,

N_f: Force carried by fibres; V_f: Volume of Fibres; A_c: Cross-sectional area of concrete; E_f: Modules of elasticity of the steel fibres; F_{yf}: Yield Strength of the Steel Fibres; ε : Strain in the reinforced concrete member; ε_y: Strain in the reinforcing bar at yielding.

Abrishami and Mitchell (1997) concluded the proposed model; Eq. [2-8] better predicts the tension stiffening response of fiber reinforced concrete. In addition, it was concluded that concrete members with fiber reinforcement showed a greater tension stiffening response compared to members without fiber reinforcement. The enhanced tension stiffening is mainly due to the fibers' ability to transfer stresses across the cracked concrete member.

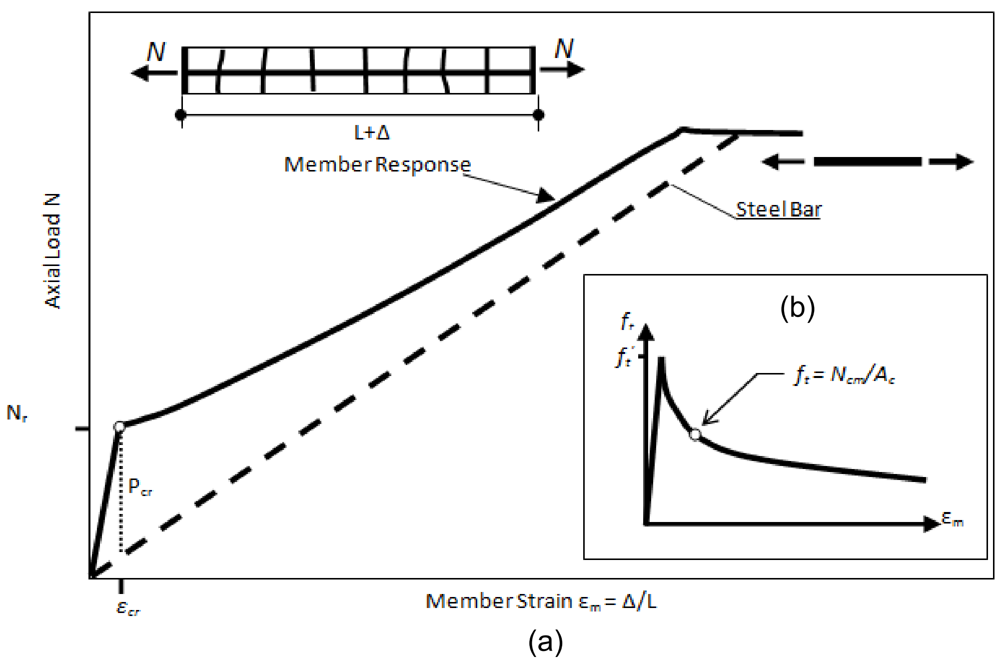

Figure 2-4 Axial Load-Deformation Response and Tension Stiffening Effect (a) Reinforced Concrete and (b) Concrete Contribution

[2.3.3] Shear Friction

Transformation of shear stress across an interface between two members that are free to move relative to each other is commonly known as the shear friction. Such behavior is generally present composite sections such as a bridge deck and the supporting beam. In order for the two sections to interact adequately sufficient shear friction is required. The basic mechanism for shear transfer test in bridge decks is summarized in Figure 2-5

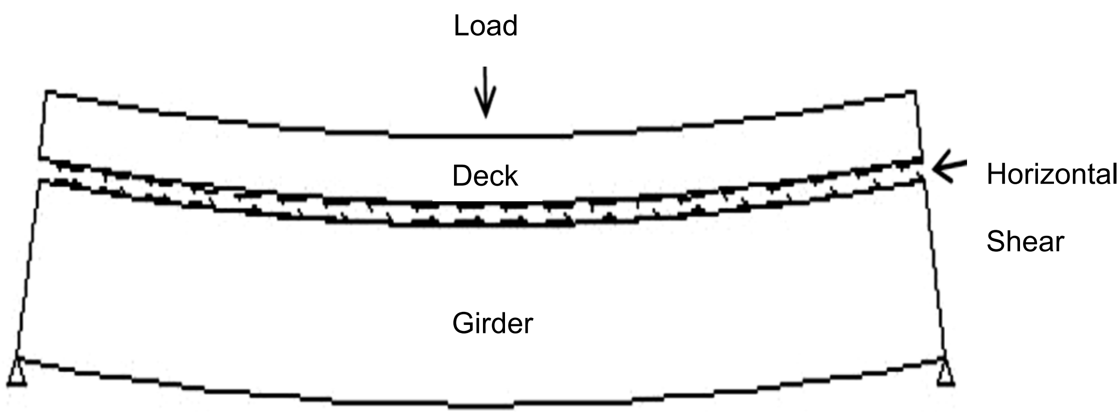

Figure 2-5 Horizontal Shear Forces in composite sections

The horizontal shear strength design criteria, clearly, depends on the design code governing the project. The current ACI-318-08 and CSA A23.3-04 provide simple design guideline, provided that the reinforcement bars are perpendicular to the shear plane, for shear friction strength of concrete, Eq. [2-9] and Eq. [2-10], respectively.

$$v_u = \mu \rho_v f_y \qquad \text{[Eq. 2-9]}$$

$$v_u = c + \mu \rho_v f_y \qquad \text{[Eq. 2-10]}$$

Where, v_u: ultimate shear stress capacity, ρ_v: shear friction reinforcement ratio, f_y: yield stress of reinforcement bar, c: 1 MPa for monolithically placed concrete, μ :1.4 for monolithically placed concrete

Throughout the years, many equations, summarized below, have been developed to adequately predict the shear friction strength of concrete. Such experiments were conducted on push specimens, where the response between the load and slip was investigated. A typical push off test specimen is illustrated in Figure 2-6

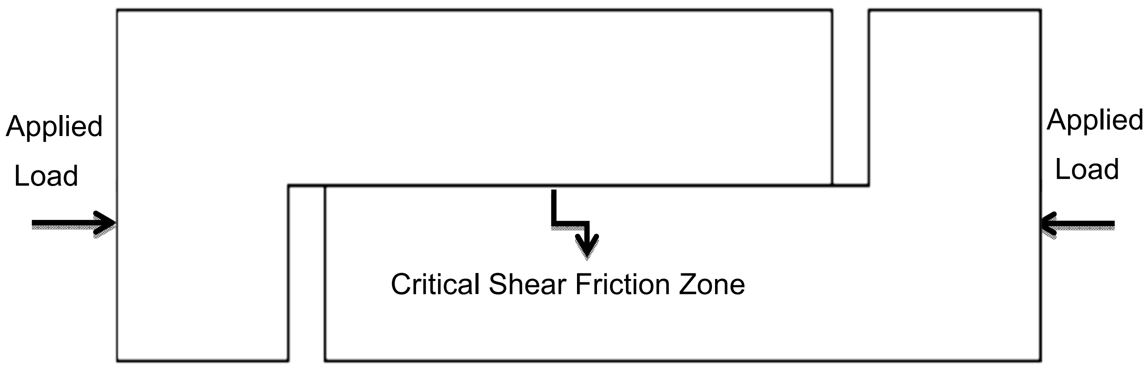

Figure 2-6 Typical Push Off Specimen

Hanson (1960): investigated the shear friction strength between precast girders and cast in place slabs. He varied the use of adhesive dong agents, keys, stirrups and surface roughness. He then concluded the base shear strength value depended on the interface treatment. Also, the addition of reinforcement added to the strength of the base shear while the variation of keys did not have an effect on the shear base.

Mattock et al (1969): studied the behavior of the shear friction of 38 different specimens to study the shear transfer behavior in interfaces where a crack existed before shear transfer. He investigated the effect of compressive strength and steel reinforcement. Mattock et al. (1969) concluded that the pre-cracked specimens resulted in lower ultimate shear strength. In addition, they reported that the concrete strength had no effect on the shear strength, and the ultimate shear friction strength was dependent on the reinforcement ratio.

Mattock et al. (1975): preformed push off test on 27 specimens to investigate the effect of moment on shear friction strength. They concluded the applied moment does not affect the transfer of shear forces. They concluded that the equation, Eq. [2-11], proposed by Mattock (1974) most accurately predicted the shear transfer.

$$v_u = 400 + 0.8\rho fy \leq 0.3 f'c \qquad \text{[Eq. 2-11]}$$

Valluvan et al. (1999): investegated the adeuacey of the shear friction strength equation as given by the ACI 318-95 of concrete placed at different times. 16 push-off tests were conducted, where they investegated the effect of reinforcement, amount of permanent compressive stress on the interface, strength of concrete and construction prodecdure. Valluvan et al. (1999),concluded that the ACI provision was rather conservative.

Khan and Mitchell (2002): preformed 50 different test on push off specimens to determine if the ACI 318 was adequate for high strength concrete. They investegated the effect of compressive strength, reinforcement ratio. In addition their tests included pre-cracked, uncracked and cold joint specimens. They concluded that the ACI 318-99 was conservative of shear friction strength of high strength concrete. They prposed the following Eq [2-12].

$$v_u = 0.05 f'_c + 1.4 \rho_v f_y \leq 0.2 f'_c \qquad \text{[Eq. 2-12]}$$

where, v_u: ultimate shear stress capacity, f'_c concrete compressive strength, ρ_v: shear friction reinforcement ratio and f_y: yield stress of reinforcement bar.

[2.4]Structural Behaviour of Concrete

[2.4.1] Shear Strength of Concrete Beams

[2.4.1.1] Background

Concrete structural elements subjected to high shear stresses are a highly sensitive topic due the complex nature of the shear behavior. Similar to the ACI-318-08, current design methods for shear capacity in the Canadian code, CSA A23.3-04 are mainly based of experimentally derived equations. Some researchers suggest using such equations might be unsafe for concrete with at least twice the strength they were developed for. Majority of the experiments were conducted on beams of a depth less than 300 mm. Previous studies on much have shown a decrease in the shear capacity of the concrete beams as the size increases (Elzanaty, 1986). This phenomenon is known as the “size effect on shear”, which simply means as a concrete beam increases in size the shear capacity decreases.

[2.4.1.2] Development of Shear design Equations

In Practice, when designing reinforced concrete members, flexural is usually considered first. The member is then, usually, proportioned for shear such that the shear strength equals or exceeds the shear required to cause flexural failure within the member. The current design equations available in design codes, ACI 318-08 and CSA A23.3-04, are a product of years or extensive research. The basis for both design equations is the product of the 45^{o} truss model analogy developed in the early 1900’s, which incorporated only the effect of the transverse reinforcement. During mid-1900’s, it then became apparent that the method was over conservative by ignoring the effect of concrete towards the shear strength of reinforced concrete section. At the time, extensive research was conducted to study the effect of the concrete on the shear strength of reinforced concrete beams. Eventfully ACI developed an empirical model to incorporate the effect of the transverse reinforcement and concrete on the shear strength. In 1955 a catastrophic shear failure collapse of a warehouse signaled the development of a more accurate shear strength model. Consequently, effortless research developed a model based on a 194 experimental data, adapted from ACI-ASCE committee 326 in 1962, summarized in Figure 2-7 (Collins and Kuchma, 1999).

During the development of the ACI shear design provision, the sensitivity of the shear failure to size and reinforcement ration was not considered (Collins and Kuchma, 1999). Concrete structural elements subjected to high shear stresses are a highly sensitive topic due the complex nature of the shear behavior.

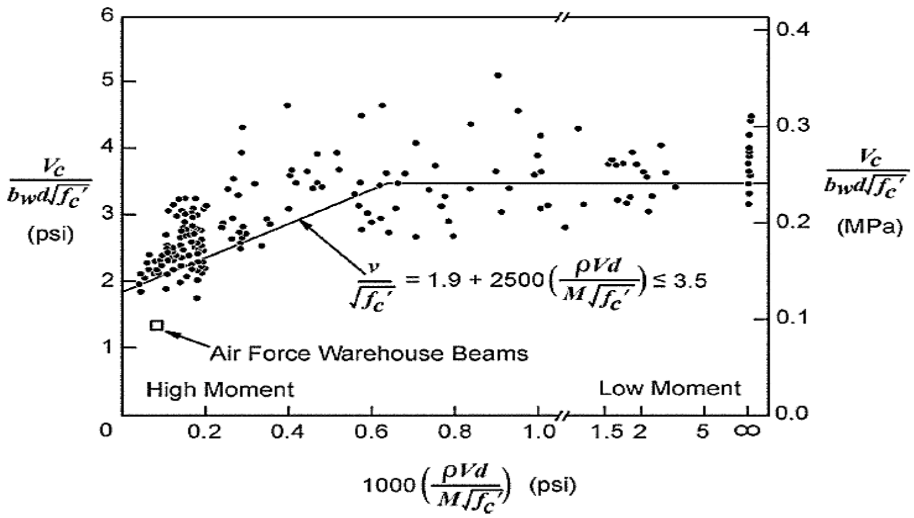

Figure 2-7 Derivation of ACI expression for diagonal cracking shear strength (Collins and Kuchma, 1999)

Similar to the ACI-318-08, current design methods for shear capacity in the Canadian code CSA A23.3-04 are mainly based on experimentally derived equations. Some researchers suggest using such equations might be unsafe for concrete with at least twice the strength they were developed for (Elzanaty, 1986). Majority of the experiments were conducted on beams of a depth less than 300 mm. In addition the code equations did not consider the size effect on beams having a depth greater than 300 mm. Beams without shear reinforcement, stirrups, will fail diagonally when an inclined crack occurs. Originally cracks vertically develop at mid-span, followed by cracks developing at approximately 1.5d (effective depth of the beam) form the face of the support. Subsequently, sudden diagonal cracks propagate towards the location of the applied load. The failure mode, described above, is more common with slender beams having a shear span to depth ratio, a/d, greater than 2. In the research at hand, the shear strength of

UHPFRC is studied while investigating effecting shear strength such as: f_c', compressive strength of concrete, *a/d* ratio and ρ_w, longitudinal steel ratio.

[2.4.1.3] Factors Effecting Shear Strength

Beams without shear reinforcement, stirrups, will fail diagonally when an inclined crack occurs. Originally, the crack vertically develops at mid-span which causes, followed by cracks developing at approximately 1.5d form the face of the support. Subsequently, sudden diagonal cracks propagate towards the location of the applied load, as shown in Figure 2-8, where ,*d*, is the effective depth of the beam and ,a, is the shear span. Figure 2-8, describes the failure mode which is associated with slender beams having a shear span to depth ratio, a/d, greater than 2. In past years countless research, (Elzanaty, 1986; Naraynan and Darwish, 1987; Ashour et al., 1992; Kwak et al. 2002; Bunje and Fehling, 2004; Concrete Committee, Japan Society of Civil Engineers, 2008 and Dibh et al. 2011), has been conducted to develop models which account for the effect associated with the *a/d* ratio. Elzanaty (1986) conducted numerous researches on the shear capacity of reinforced concrete beams using high strength concrete. The research was focused on testing the adequacy of the ACI 318-08 shear design equation, Eq. [2-3] (ACI Committee 363 R, 2010), when using high strength concrete. During the research, Elzanaty (1986) focused on parameters affecting shear strength such as; concrete compressive strength f_c', a/d ratio and longitudinal steel ratio ρ_w. Elzanaty (1986) then concluded; the shear strength of beams without stirrups increased with the increase of concrete strength. However, the ratio of the test to the predicted shear strength decreased with the increase of concrete strength. ACI 318-10, Eq. [2-13], was seriously unconservative for beams without stirrups having a high f_c' and a/d ratio with lowρ_w.This code equation underestimates the importance of both ρ_w and a/d ratio and overestimates the benefit of increasing f_c'. The Canadian concrete design criterion, CSA A23.3-04 follows similar guidelines to the ACI 319 and is represented with Eq. [2-14].

$$v_c = 1/6\sqrt{f_c'}\ (MPa) \qquad \text{[Eq. 2-13]}$$

$vc = \lambda\beta\sqrt{fc'}$ *(MPa)* [Eq. 2-14]

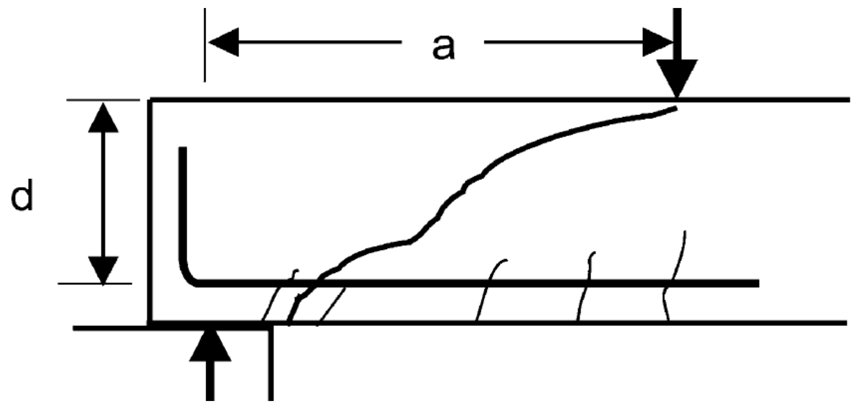

Figure 2-8 Development of a Shear Crack

[2.4.1.4] Shear Strength of Fibre Reinforced Concrete

The addition of randomly integrated steel fibres in concrete has been commonly known to enhance the behaviour of conventional concrete. The development of the fibre reinforced design models dates back at least 30 years ago (Kwak et al., 2002). Since, a number of models have been developed to accommodate the presence of steel fibres in concrete.

Sharma (1986), developed a simple model to predict the shear strength of fibre reinforced concrete beams represented by Eq. [2-15].

$vu = k\ ft'(d/a)0.5$ *(MPa)* [Eq. 2-15]

where v_u: average shear stress at failure, k: 2/3, a/d: shear span-depth ratio, f_t': split-cylinder tensile strength or $0.79(f_c')^{0.5}$ and f_c': concrete compressive strength.

However, the model fails to take into account major parameters influencing the shear strength such as flexural reinforcement ratio and fibre reinforcement. Following the development of Eq. [2-15], many other models were developed for shear strength design of fibre reinforced concrete. Narayanan and Darwish (1987) developed a shear strength model accounting for fibre and flexural reinforcement given by Eq [2-16]. Ashour (1992) modified Eq. [2-16] to better fit his result from high strength concrete beam subjected to shear experiment. His model, Eq. [2-71], directly includes the most important parameters affecting shear strength such as reinforcement ratio, shear span to depth ratio (a/d) and concrete strength and compressive strength. Using the results of his own experiment and those of Ashour (1992) and Narayanan and Darwish (1987), Kwak et al. (2002) developed an additional model for shear strength of fibre reinforced concrete, Eq [2-18].

$vu = e[0.24\, f_{spfc} + 80\rho \frac{a}{d}] + vb$ (MPa) [Eq.2-16]

$vu = (0.7\sqrt{fc'} + 7F)\frac{d}{a} + 17.2\rho \frac{d}{a}$ (MPa) [Eq.2-17]

$vu = 3.7e\, f_{spfc}^{2/3} (\rho \frac{d}{a}) 1/3 + 0.8vb$ (MPa) [Eq.2-18]

Where, $f_{spfc} = f_{cuf} /(20-\sqrt{F}) + 0.7 + \sqrt{F}$, ρ: flexural reinforcement ratio, a/d: shear span-depth ratio, F: fibre factor $(L_f/D_f)V_f d_f$, e: arch action factor (1 for a/d> 2.8, 2.8for a/d<2.8), f_{cuf}: concrete compressive strength, L_f : fiber length, D_f: fibre diameter V_f: volume fraction of steel fibers and d_f: bond factor (0.5 for round fibers and 0.75 for crimped fibres), v_b: 0.41TF, T: average fiber matrix interfacial bond stress, taken as 4.15 MPa

The previous models, though very effective when using high strength fibre reinforced concrete, have yet to be verified for use with UHPFRC. The Japan Society for Civil Engineers is one of the few organizations to develop design recommendations for structure members made with UHPFRC. Eq [2-19] (Concrete Committee, Japan Society of Civil Engineers, 2008), predicts the shear capacity of concrete members made with fibre reinforced concrete and without stirrups where, V_{cd} is the effect of concrete and V_{fd} is the effect of fibre reinforcement.

$V_{yd} = V_{cd} + V_{fd}$ (N) [Eq. 2-19]

Where,

$V_{cd} = \beta_d * \beta_p * f_{vcd} * b_w * d/\gamma_b$

V_{fd}= (f_{vd}/tan β_u)*b_w* z/ γ_b

Where, β_d = $\sqrt[4]{1/d}$, β_p = $\sqrt[2]{100/\rho w}$, f_{vcd} = 0.7 * 0.2* $\sqrt[3]{f_{cd}}$, ρ_w: flexural reinforcement ratio, b_w: beam width, d: effective beam depth, z: distance from location of compressive resultant to centroid of tensile steel, generally d/1.15, γ_b: 1.3 in general, f_{vd}: design tensile strength of UHPFRC,β_u: angle of diagonal crack surface to the member axis, β_u = 45^0

Later research has linked the shear strength of fiber reinforced concrete directly to the fiber reinforcement rather than the tensile strength of concrete (Aoude et al., 2012). To illustrate the propoed concept behind this approach, a free body diagram of fiber reinfored concrete beam with a crack inclination, θ, as shown in Figure 2-9 can be considered. The shear resistance, V_{fib} , can be related to the pullout strength of the fiber reinforcement as shown in Eq. [2-20] (Aoude et al., 2012).

V_{fib} = *[N_{fib} (0.83 F_p)] b_w d cot* θ [Eq. 2-20]

The effective number of fibers N_{fib} can be calculated based on the fiber volume fraction of the concrete. The number takes into account the fiber orientation (α=3/8) and the embedment length of the fiber (η_l = ½). The fiber pullot strength, F_p, takes into account the yielding strength of the fibers as well as the fiber type. Results have shown fiber with hooked end tend to increase the pullout strength due to the anchorage provided by the hooks. Aouda et al. (2012) showed excellent correlation between the test results and the model proposed for shear strength.

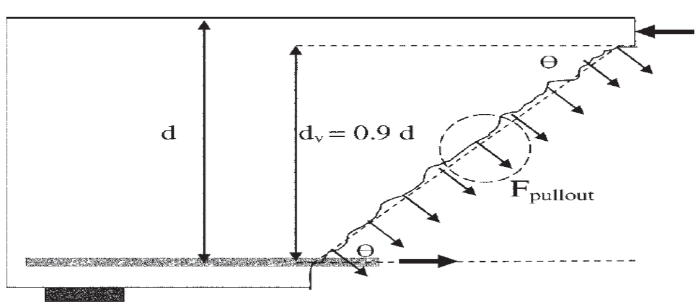

Figure 2-9 Fiber pull off Resistance Contributing to Shear Strength

Chapter [3]
Experimental Procedure

[3.1] Introduction

The rapid increase in using UHPFRC in today's industry triggered the need for design guidelines incorporating the effect of fibre reinforcement. While research facilities across the globe have produced UHPFRC with compressive strength ranging from 100-800 MPa (ACI Committee 363R, 2010); the only commercially available UHPFRC in North America is produced by Lafarge North America. Ductal©, a brand of UHPFRC, utilizes steel or organic fibres, as part of the concrete mix design, to increase the ductility and enhance the post cracking behaviour. The focus of the research at hand is to investigate the structural properties of Ductal©, with steel fiber reinforcement, to determine the adequacy of such material in today's industry. Table 3-1 Summarizes the properties of the UHPFRC used throughout the course of the research presented. It should be noted, the research presented only includes the UHPFRC made with metallic (steel) fibres

Table 3-1 Mechanical Properties of Ductal© (Lafarge North America, 2011)

	Metallic Fibres	Organic Fibres
Density	2500kg/m3	2350kg/m3
Compressive Strength	150-180 MPa	100-140 MPa
Flexural strength	30-40 MPa	15-40 MPa
Direct Tensile Strength	8 MPa	5 MPa
Young's Modulus	50 GPa	35 GPa
Poisson Ratio	0.2	0.2
Shrinkage	0.6-0.8 mm/m	0.8-1 mm/m
Creep Coefficient	0.3	0.8
Coefficient of Thermal Expansion	11.8 550 μm/m/C	11.8 550 μm/m/C

[3.1.1] Fiber Reinforcement

The steel fibers used in all the experiments were straight fibers with a diameter of 0.2 mm and length of 12 mm. In addition the fibers are coated with a thin layer of brass to prevent rusting during storage and handling. The material property of the fibers used in outlined Figure 3-1.

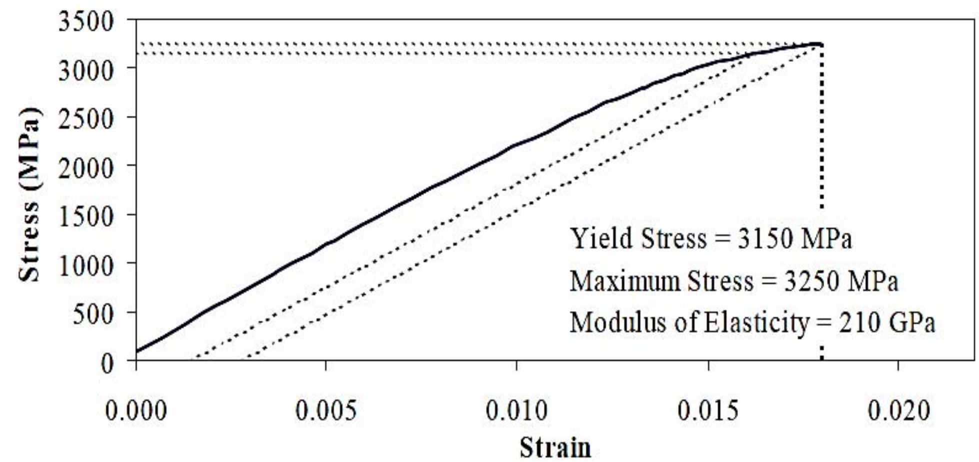

Figure 3-1 Material Properties of Steel Fibers (Federal Highway Administration, 2006)

[3.1.2] Mixing Procedure

The mixing efficiency and mixing performance depends highly on the mixing procedure and mixer type. For the most efficient and consistent mixing of UHPFRC shear mixers have been used successfully. These mixers disperse the water and admixtures onto the cement without heating the mix via kinetic energy created by the mixing process. The mixing procedure was done according to Lafarge North America specification for producing Ductal© concrete. The dry material, consist of a carefully selected blend of nano materials such as cement slag silica fumes and silica sand, was mixed first, to allow even distribution of raw materials. Following the dry mix, water and high end water reducer admixture were gradually added to the dry materials. Afterwards, when the mix reached the desired consistency the steel fibres were evenly added to the mix. The exact proportions of the mix design and the duration of the mixing procedure cannot be disclosed due to confidential agreement with Lafarge North America.

[3.1.3] Casting

After the completion of the mixing, the concrete was then transported via plastic buckets to be poured. Prior to pouring of the concrete the formwork were cleaned thoroughly then the sides were slightly oiled to ease the demolding process. When UHPFRC is discharge onto a flat surface, UHPFRC spreads itself throughout the mold. By moving the discharge point at a rate such that it is always behind the leading edge of the flow the mold can be filled in one continues motion. This casting technique is rather important, because if two leading edges meet there will be minimum fibers available to bridge the two edges. Due to the self-consolidating and self leveling properties of Ductal© concrete the need for vibration was eliminated.

[3.1.4] Curing

UHPFRC requires a different curing method when compared to conventional concrete. All test specimens were cured according to Lafarge North America curing specification for Ductal© concrete. The specifications require the placement of a plastic layer over the concrete specimen after the addition of fresh water to the surface of the concrete,

Figure 3-2 Typical Test Specimen While Curing

[3.1.5] Compressive Strength Testing

Following the casting of each specimen, a minimum of three compressive strength test cylinders were cast. The cylinders were tested on the same day as their respected test specimen. Unlike conventional concrete, the use of capping compound, to achieve a uniform test surface, is not suitable for UHPFRC. The expected compressive strength of the UHPFRC (150-180 MPa) is greater than the compressive strength of the capping compound (80-90 MPa). As an alternative, the uniform test surface was achieved using a concrete saw as shown in Figure 3-3.

(a) (b) (c)

Figure 3-3 (a) Typical Test Cylinder after Demolding, (b) While Saw Cutting and (c) After Saw Cutting

[3.1.6] Reinforcing Steel

The reinforcement bars used throughout the experiments were grade 400 MPa (10 mm) and 450 MPa (20 and 25 mm) Canadian steel bars conforming CAN/CSA-G40.20-M92. The reinforcement consisted of deformed bars 10 mm, 20 mm, 25 mm, in diameter; with average yield stress and ultimate tensile strength of 425 MPa. The steel bars had a modulus of elasticity of 200 GPa. Details of bar size, spacing and arrangements are outlined in the following sections.

[3.1.7] Measurement Devices

[3.1.7.1] Load Measurement

Two methods of load application and measurements were used in the course of the experiments. The first method was by means of a hydraulic pump used to apply the load that was then measured by a hydraulic pressure transducer. The transducer was connected to a high speed data acquisition system. As for the second method, a Material Testing System (MTS) equipped with load, strain and deflection loading rates. A high speed data acquisition system was used. The details of which method used will be outlined in following sections.

[3.1.7.2] Strain Gauges

Two types of strain gauges were used throughout the course of the experiment. The traditional electrical strain gauges (ESG), 10 mm long, with a resistance of 120 Ω and a gauge factor of 2.07±0.5%, were glued to steel reinforcing bars. The gauges were installed according to specifications. Initially the bar was grinded to achive a smooth and even surface without compromising the carrying capacity of the bar. Then a alcohol is applied to the smooth surface to clean the contaminated surface. Afterwards, a coditional is applied to the surface and then the strain gauge in glued to the steel bar. The other type of strain gauges used was a Fiber Optic strain sensor. Fiber Brag Grating (FBG) sensors are one of many fiber optic sensor technologies that are currently being used in SHM systems. A fibre Bragg grating is wavelength-dependent filter/reflector formed by introducing a periodic refractive index structure, with spacing on the order of a wavelength of light, within the core of an optical fibre. Whenever a broad-spectrum light beam impinges on the grating, it will have a portion of its energy transmitted through, and another reflected off. The reflected light signal will be very narrow (few nm) and will be centered at the Bragg wavelength that corresponds to twice the periodic unit spacing. Any change in the modal index or grating pitch of the fibre caused by strain, temperature, displacement, or cracks in buildings will result in a Bragg wavelength shift. An FBG is a region of germanium-doped glass fibre core that has been exposed to UV radiation using a ‘phase mask’ to fabricate a periodic ‘grating’ of material with a modulated index of refraction. This precise spacing, called the ‘pitch’, reflects incident light in a narrow band centered about the ‘Bragg’ wavelength.

The electrical strain gauges (ESGs) are susceptible to Electromagnetic or radio frequency interference (EMI/RF) and hence unsuitable for long-distance applications. Structurally, each ESG has two wires serving as input and output ports respectively, unlike fiber Bragg grating based sensors where several sensors can be multiplexed onto the same optical fiber. Consequently, FBG sensors could allow for a larger and a more accurate measurement for the fracture and cracking response of concrete members. Figure 3-4, shows a typical Fiber Optics sensor installed. The details of which type of strain gauge used will be outlined in sections to follow.

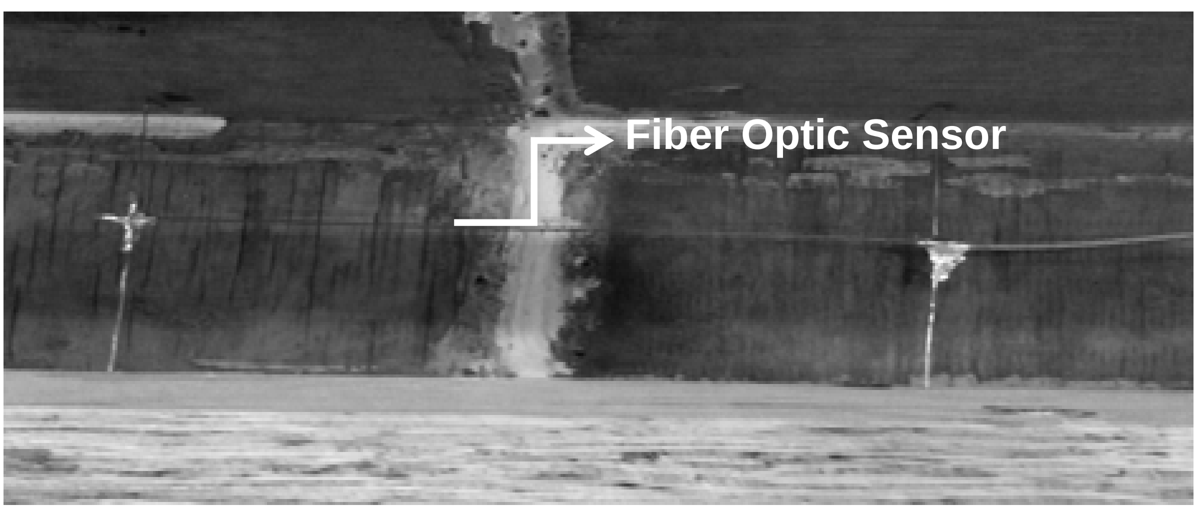

Figure 3-4 Typical Fiber Optic Strain Sensor

[3.1.7.3] Deflection Gauges

The deflections were measured using an assortment of linear potential differential transducers (LPDTs), outlined in detail in the following sections. LPDTs work on the basis of linear relationship between the resistance and displacement due to deflections or deformations occurrence.

[3.2] Fracture Energy Testing

[3.2.1] Specimen Specification

A total of two identical specimens were cast for fracture energy determination as outlined in Table 3-2. The specimens were tested under a four-point loading system using the MTS machine outlined above. The two specimens were identical in details to verify the results of the experiment.

Table 3-2 Fracture Energy Test Specimen Specification

Specimen Name	Cross Sectional Area (mm^2)	Length (mm)	Notch Depth, a_0 (mm)
FE1	200x300	900	40
FE2	200x300	900	40

Following the mixing, the concrete was then transported, in plastic buckets, to be cast in wooden molds previously prepared. The molds had dimension of 200 x 300 x 1000 mm. prior to casting, an artificial notch with depth of a_0 = 40 mm along the width of the specimen was prepared at the middle of the specimen as shown in Figure 3-5. In addition, to measure the strain along the fracture zone, a fibre optic strain gauge, 150 mm, was installed. The specification of the test specimens are shown in Figure 3-6.

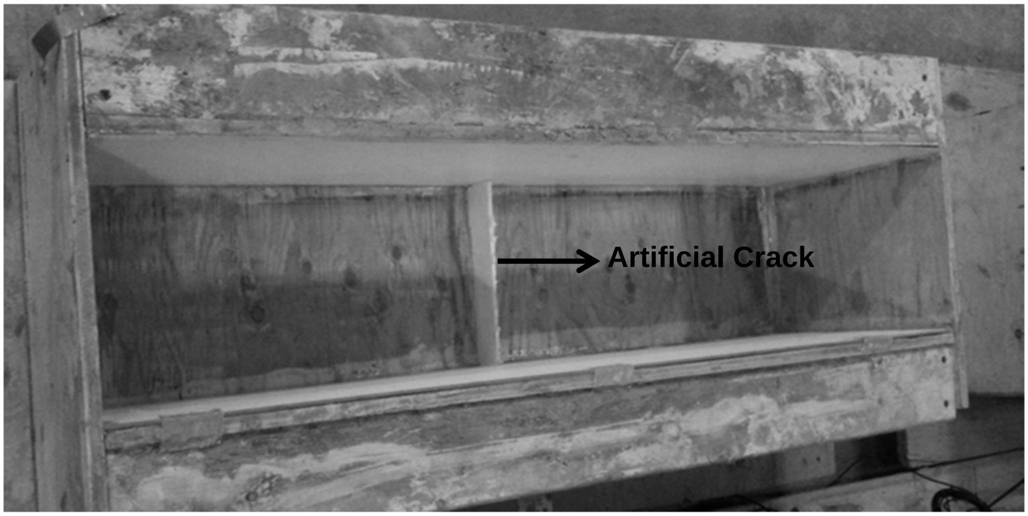

Figure 3-5 Artificial Crack

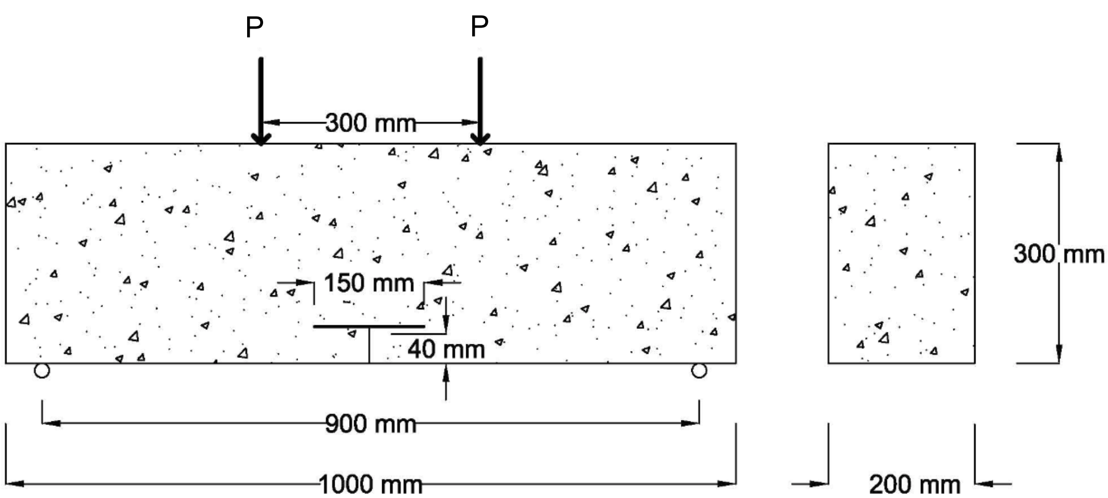

Figure 3-6 Overview of Fracture Energy Test Specimen

[3.2.2] Testing Procedure

Literature review suggests strain or deflection control loading rate to correctly capture the fracture energy of concrete (Marzouk and Chen, 1995). The testing apparatus used to apply the load in this experiment is capable of controlling the load, strain and deflection loading rate. As for the strain measurements a separate acquisition system was used to capture the change in wavelength from the fibre optics cable, with a gauge length of 150 mm, which then can be used to calculate the strain along the cable. Both acquisition systems were adjusted to record measurements at a rate of 4 readings per second. Figure 3-7 below shows the experimental test setup. The experiment was conducted under a displacement loading rate of 0.0004 mm/s. Based on the results and the behavior observed from first test Specimen, the loading rate was increased to, 0.008 mm/s, as it became evident that a slow rate is not required as the specimen showed a ductile behaviour.

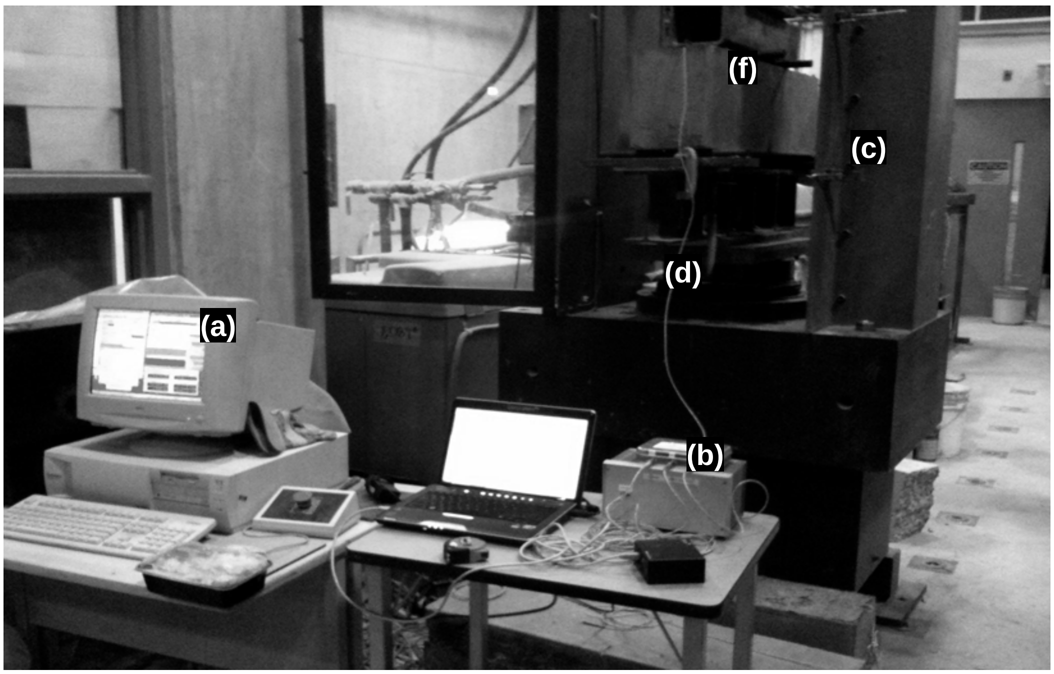

Figure 3-7 Fracture Energy Test Setup and Instrumentation (a) Acquisition system, (b) Fibre optic wavelength acquisition system, (c) MTS Machine, (d) Fiber Optic Cable and (f) Test Specimen

[3.3]Tension Stiffening

[3.3.1] Specimen Specification

Two test specimens were cast to determine the tension stiffening behaviour of UHPRFC. The effect of reinforcement ratio was investigated by varying the cross-sectional area of the specimen. The detailed specimen's specifications are presented in Figure 3-8 and

Table 3-3.The steel reinforcement used was longer than the test specimen to ease in the testing procedure detailed in the following section.

Table 3-3 Tension Stiffening specimen Details

Specimen Name	Cross Sectional Area (bxb mm2)	Length, L (mm)	Reinforcement Ration (%)
TS1	180x180	2000	1.5
TS2	160x160	2000	2

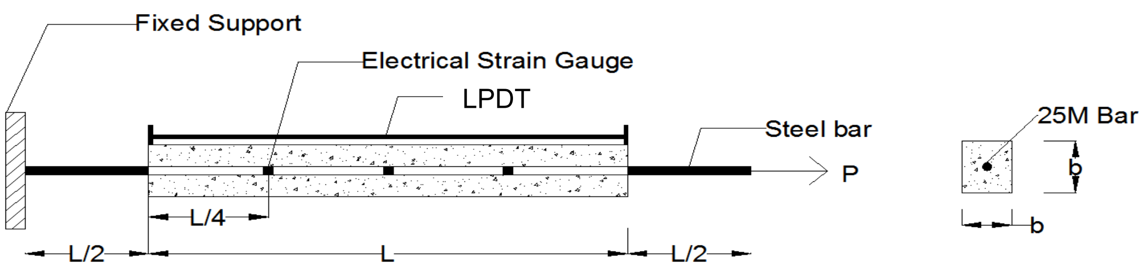

Figure 3-8 Tension Stiffening Specimen Specification

[3.3.2] Testing Procedure

A special test set up was assembled to create a fixed connection at one end of the test specimen and apply a horizontal load to the specimen. The setup, consisted of two steel frames, mounted into the floor, and two reinforcement grips to create a fixed connection and apply the load. The extended reinforcement bar was placed, on either side, through the steel frame which was then mounted to the ground. On one side the steel bar was placed through a hollow hydraulic jack and a hollow load cell then mounted to the reinforcement grip as illustrated in Figure 3-9 (a). On the other side the steel bar was mounted to the steel grip to restrict any horizontal movement due to the load applied, creating a fixed connection, Figure 3-9 (b).

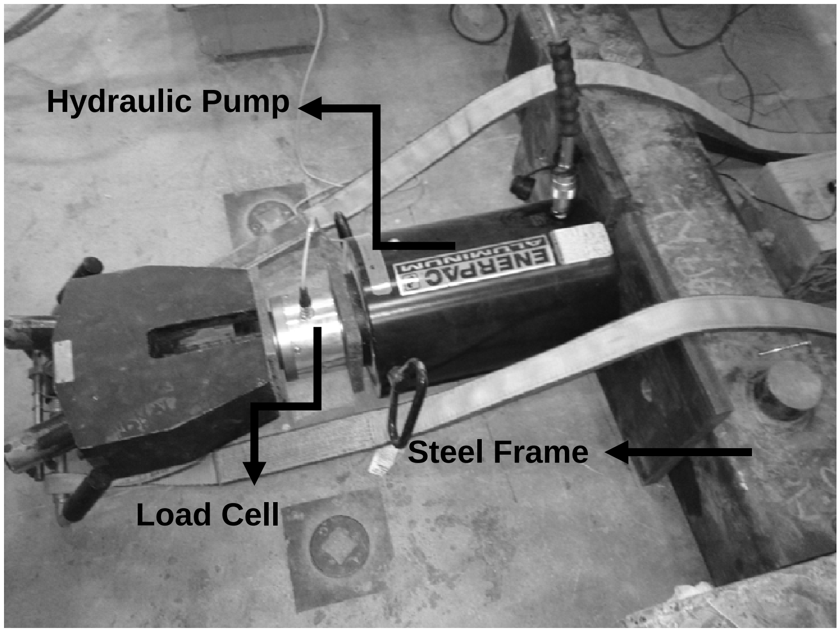

(a)

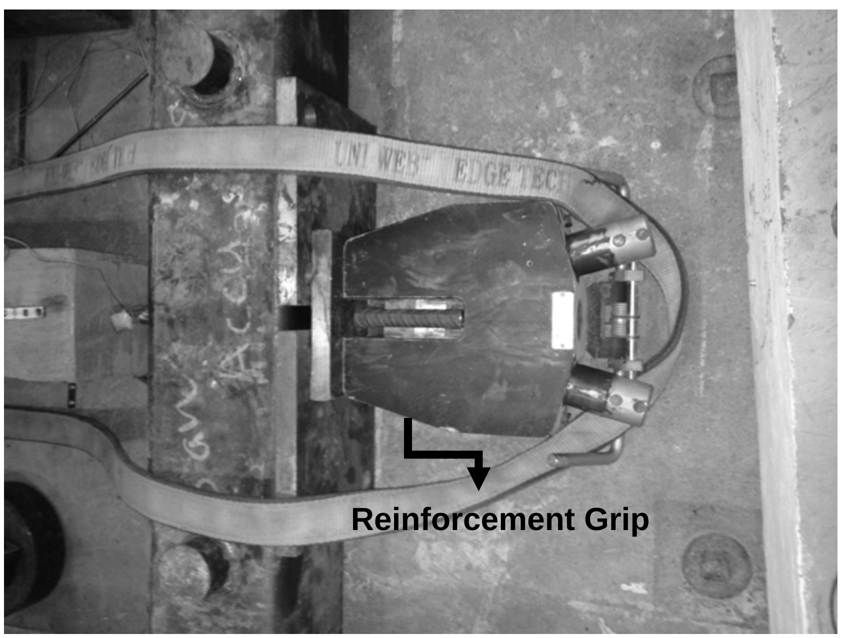

(b)

Figure 3-9 Tension Stiffening Test Setup (a) Load Application and (b) Fixed Connection

To prevent the steel frame from horizontal movement, additional steel beams were placed between the steel supports. To measure the strain in the concrete, a LPDT deflection gauge was mounted on the specimen prior to testing. The test was conducted under a static load application and the load was applied by 25 kN increments, and any cracks developed were marked accordingly. An overview of the test setup is shown in Figure 3-10.

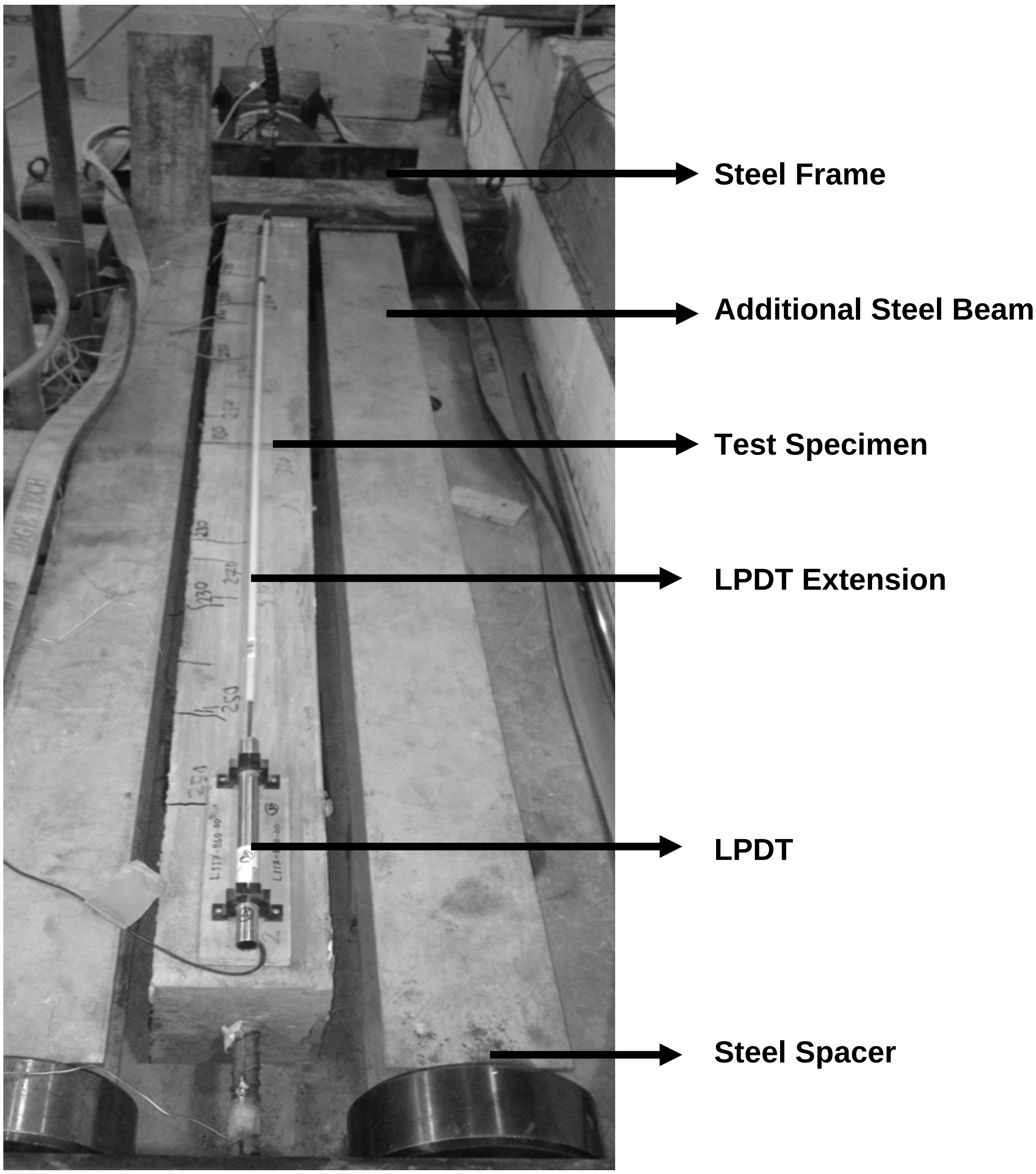

Figure 3-10 Overview of Tension Stiffening Test Set Up

[3.4] Flexure and Shear Behaviour of UHPFRC Beams

[3.4.1] Specimen Specification

A total of five beams were casted to investigate the flexure and shear behaviour of UHPFRC. All beams, outlined in Table 3-4 and Figure 3-11, were tested under a four-point loading symmetrical system. Five Strain gauges were affixed to the reinforcing bars, at L/6 spacing, to monitor the strain due to the applied load at various locations. In the case of the control beam with no reinforcement bars, SB1, a fiber optic strain gauge was used to monitor the strain variation. In addition, three LDPTs gauge were mounted to measure the deflection of the beam at a spacing of L/4.

The beams were designed to investigate the influence of reinforcement ratio, ρ_w, and the Shear span ratio (a/d) on the structural response of the reinforced UHPFRC beams. A detailed specification of the test specimen is presented in Figure 3-11.

Table 3-4 Specification of UHPFRC Beams

Beam Name	Span, L (mm)	Cross section (mm2)	Shear span ratio, a/d	Steel Ratio, ρw
SB1	1830	178x305	2.3	0
SB2	1830		2.3	1.25
SB3	3660		4.6	
SB4	1830		2.3	2.5
SB5	3660		4.6	

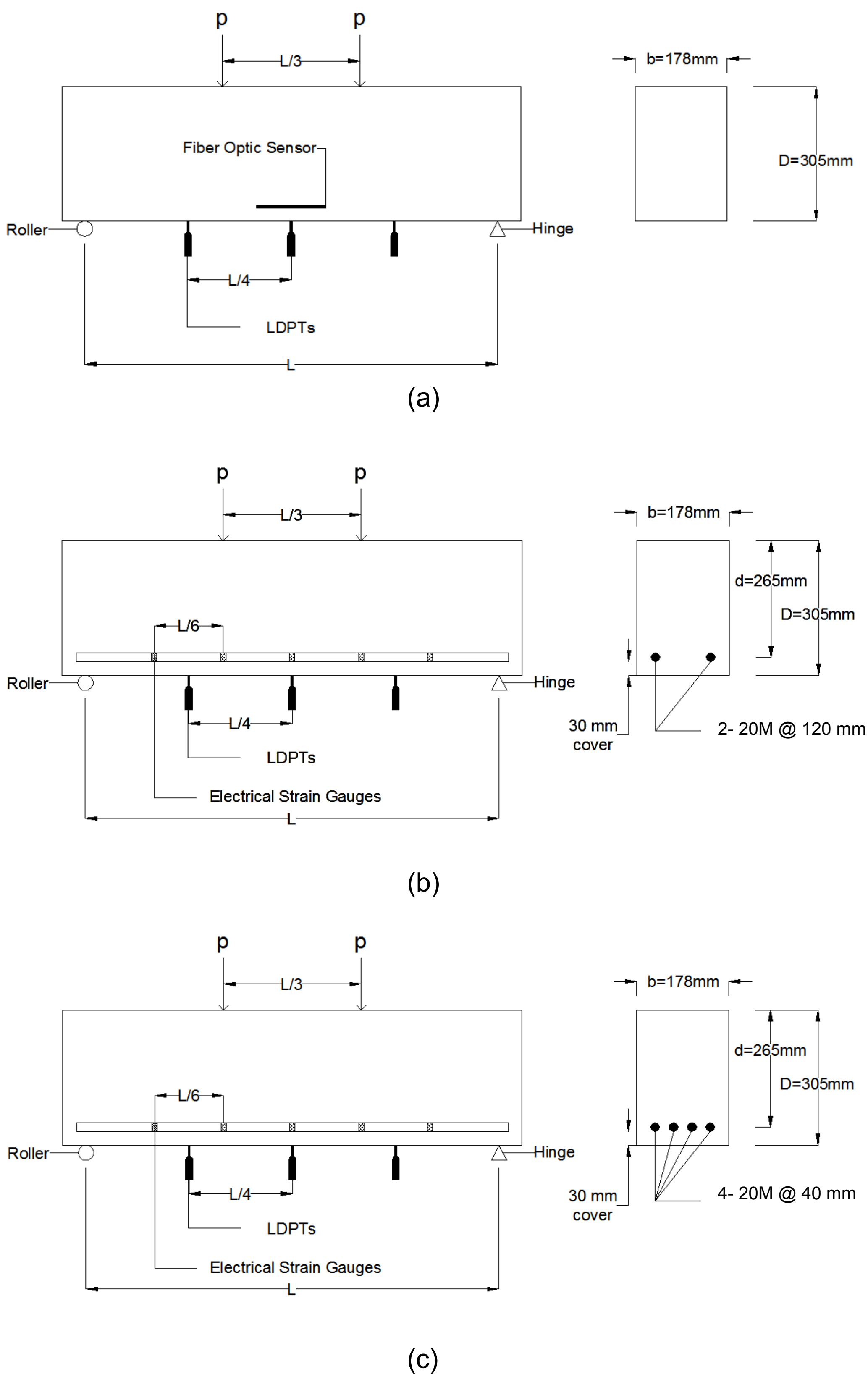

Figure 3-11 Detailed Beam Specification (a) SB1, (b) SB2&3 and (c) SB 4&5

[3.4.2] Testing Procedure

During the testing procedure, the beams were loaded by approximately 20 kN increments. Between the loading increments the beams were inspected for any cracks initiated and accordingly marked. Also, all acquisition systems were programmed to record readings at a rate of 10 readings per second. In all the beams tested the maximum load was obtained far after yielding of reinforcement bars. Test beams were considered “failed” when it was no longer possible to apply load. Figure 3-12 shows a typical beam testing setup.

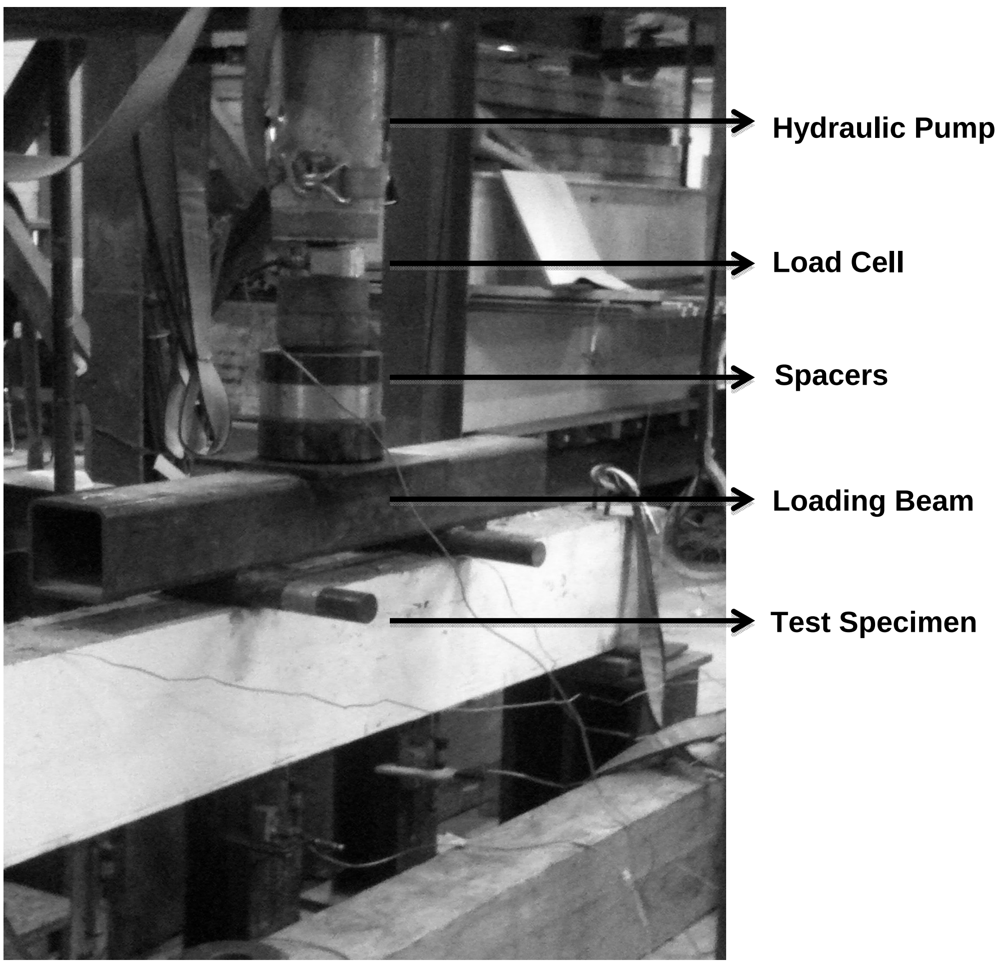

Figure 3-12 A Typical Beam under Four Point Loading

[3.5]Shear Friction

[3.5.1] Specimen Specification

Three push off test specimens were cast to investigate the shear friction properties of UHPFRC. The specimens were designed to be nearly identical to specimens designed by Khan and Mitchell (2002) so that the result could be later compared with results for normal and high strength concrete. The specimens were designed to investigate the effect of transverse reinforcement ratio on the shear friction of UHPFRC. Three different shear reinforcement ratios, $\rho_{v,}$ were used as specified in Table 3-5. To resist the moment created on the specimens due to the vertical load applied, heavy flexural reinforcement is provided to ensure shear failure as shown in Figure 3-13.

Table 3-5 Push Off Test Specimens Specification

Specimen Name	Shear Area (mm^2)	Steel Ratio ρ_v (%)
SF1		0
SF2	305x101.5	0.5
SF3		1

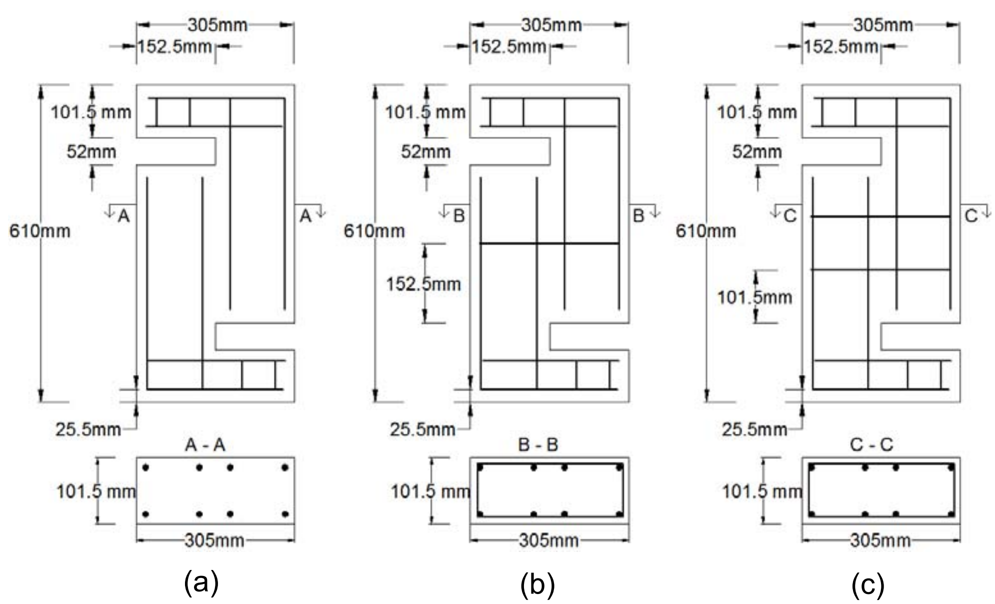

Figure 3-13 Reinforcement Detailing for Push off Specimens (a) SF1, (b) SF2 and (c) SF3

[3.5.2] Testing Procedure

The test was conducted using a MTS machine capable of load and deflection loading rates. During the testing procedure, the specimens were loaded, vertically, by approximately 10 kN increments. Between the loading increments the specimens were inspected for any cracks initiated and accordingly marked. Furthermore, all acquisition systems were programmed to record readings at a rate of 10 readings per second.

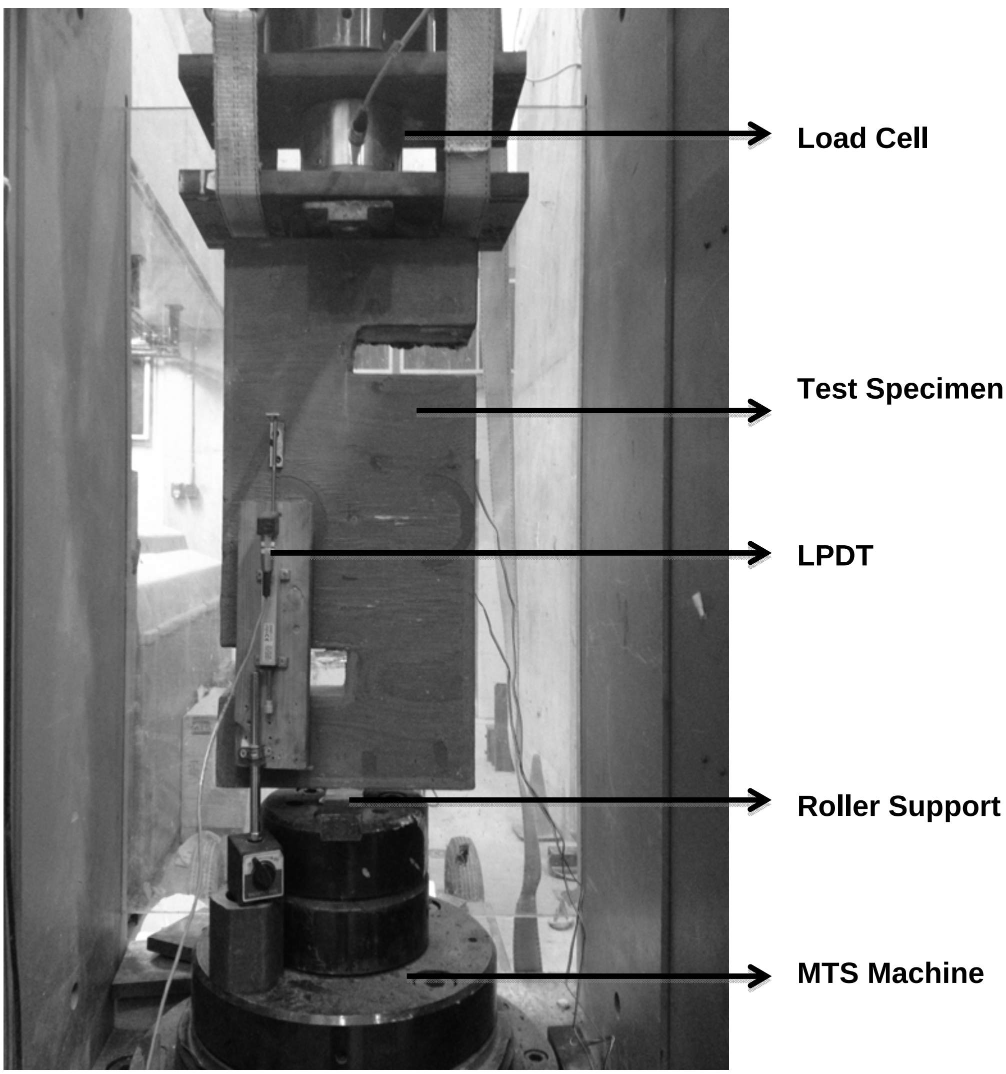

Figure 3-14 Overview of Push-Off Specimen Test Set up

Chapter [4]

Analysis of Mechanical Properties

[4.1] Introduction

This Chapter presents the results and observations of the experiments presented in Chapter 3. The effects of investigated parameters are discussed in details in the following sections. The load response behaviour of each test is presented then analysed and compared to previous research available in the literature.

[4.2]Fracture Energy

[4.2.1]Results and Observations

In general, concrete is a brittle material thus making the capturing of a complete load-deformation response a problematic task. However, when using fiber reinforced concrete, the addition of the steel fibre matrix allows the concrete to behave with a more ductile behavior. Consequently, the load-deformation is easily captured. Figure 4-1 and Figure 4-2 below, illustrate the load strain relationship of the tested beams FE1 and FE2. Figure 4-1, shows the the load strain increased proportionally up to approximately 90% of the ultimate load, P_u. Afterward, the strain increased dramatically while a minor increase in the load was observed, explained by the pulling out of the steel fibres present at the crack location.

In all tested beams, surface cracks were observed at approximately 80-90 % of the ultimate load, Figure 4-3. Subsequently, the strain gradually increased as the load decreased corresponding for crack opening. However, internal cracks formed far before reaching the 80-90% of the ultimate load stage. The micro cracking can be described by the slope change in the load-strain response summarized in Figure 4-1. These, internal cracks, would immediately propagate to the surface in the case of non fiber reinforced concrete. Nevertheless, one of the main advantages of using UHPFRC is that cracks are sealed and held tightly by the steel fibres present in the concrete mix.

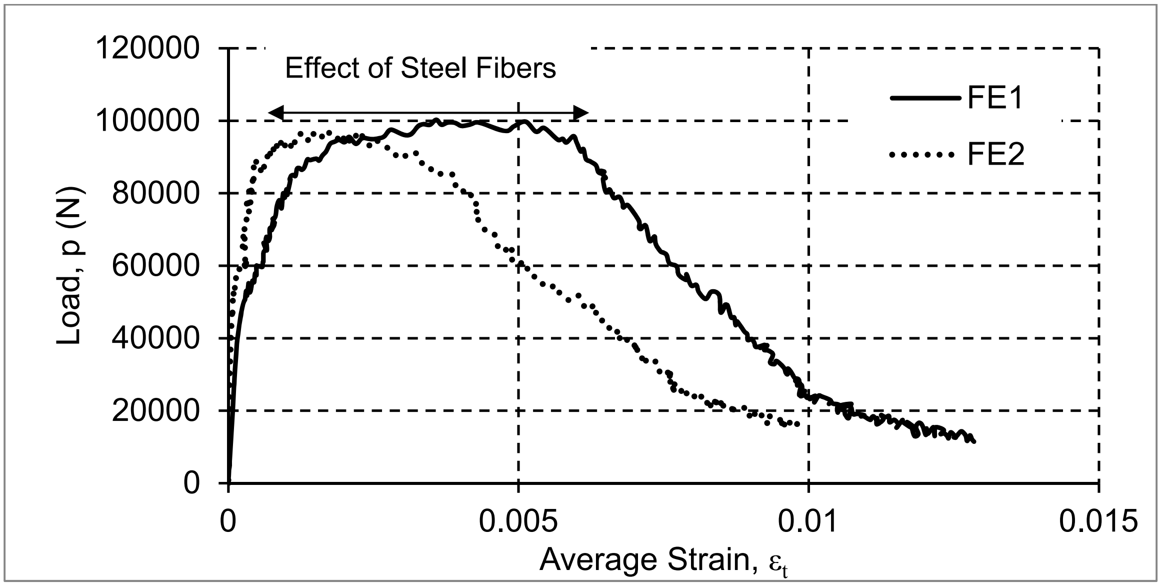

Figure 4-1 Average Strain Measurement of beams FE1 and FE2

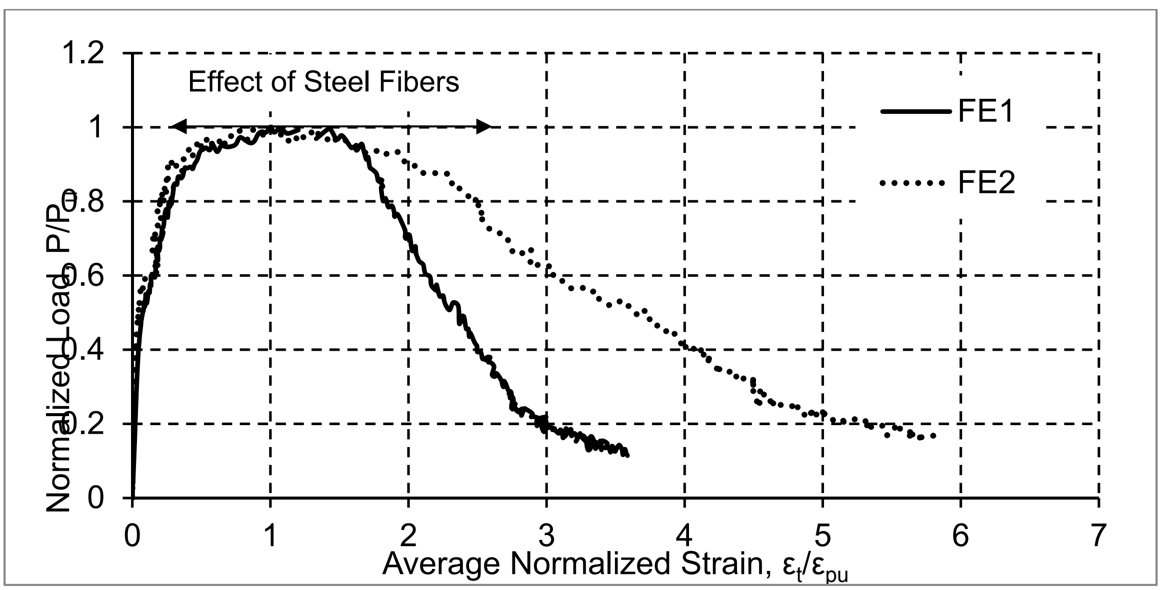

Figure 4-2 Average Normalized Strain Measurements of Beams FE1 and FE2

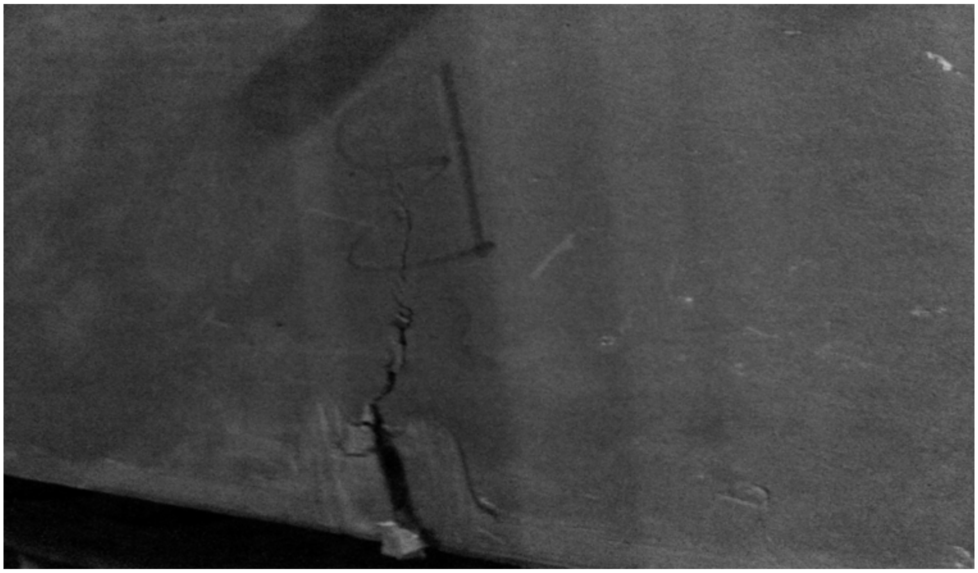

Figure 4-3 Crack Development during Fracture Energy Testing, FE2

[4.2.2] Analysis and Discussion

Fracture energy is the energy required to form a unit area of crack surface (Hillerborg , 1985). Many researchers suggest that the fracture energy of concrete be treated as a material property. Fracture energy, G_F, is considred to be the area under the stress-crack mouth opening displacement (CMOD) curve (Marzouk and Chen, 1995). However, when dealing with concrete, unlike metal, the energy absorbed by conctere is only assoiated with the area under the decending portion of the stress-CMOD curve (Marzouk and Chen, 1995). It must be noted that the effect of the steel fibre, Figure 4-1, must also be included in the fracture energy, as it ultimately gives UHPFRC its high compressive and tensile strength which are prameters that affect the fracture energy.

The maximum effective strain, ε_{max}, for HSC is reported to be around 16 times the strain at ultimate load (ε_p), (Marzouk and Chen, 1995). However, when using UHPFRC it is observed that ε_{max} is much greater than ε_p, due to the high ductility. The fracture energy can then be claculated using the load-CMOD response in accordance with Eq. [2-2].Table 4-1 summarizes the mechanical properties of the test specimens.

Table 4-1 Fracture Energy Test Results

Specimen Name	f_c' (MPa)	P_u (kN)	ε_{pu} x 10-6	ε_{cr} x 10-6	G_F (N/m)	E_t (GPa)	f_t' (MPa)
FE1	163	100.25	3500	300	1483.94	18	8.68
FE2	137	97.5	1700	135	1567.50	57	8.44

In general, fracture energy increases with the increase of the maximum coarse aggregate size; due to the increased compressive strength. However, such an observation can not be applied to UHPFRC since there is no coarse aggregate present. One,could make the argument of the fibre content having a signicicant effect on the fracture energy. The fiber content has a significant effect on the load-CMOD relation; increasing the CMOD values significntly to those of normal or high strength concrete. The fracture energy, G_F, of normal and high strength concrete, based on a direct tension test, are 110 N/m and 160 N/m respectively (Marzouk and Chen, 1995). The effect of the fibres is reflected in the high fracture energy values, as presented in Table 4-1. It was observed that UHPFRC yield fracture energy values much greater than those of normal and high strengh concrete. It was found, on average, UHPFRC yields a fracture energy value 10 times greater than normal or high strength concrete.

Rather than the use of fracture energy directly in any design models developed; the characteristic length, $l_{ch,}$ material property representing the size of the fracture zone, is used. It expresses the fracture properties of concrete such as the modulus of elasticity, E_c; fracture energy, G_F; and tensile strength, f_t as determined by the direct tension test (Hillerborg , 1985) and is represented by Eq [4-1]. While, l_{ch}, has no physical meaning; it act as a representation of the brittleness of concrete, the higher the l_{ch} value the less brittle the concrete.

$$l_{ch}=E_c\, G_F/ f_t^2 \quad (mm) \qquad \text{Eq. [4-1]}$$

Where, l_{ch} : the characteristic length; G_F : the fracture energy, E_c : the modulus of Elasticity and f_t^2 : the maximum tensile strength.

Given the difficulties associated with fracture energy determination of concrete, researches have proposed empirical equations to predict the characteristic length of concrete using the compressive strength of concrete, as presented by Eq. [4-2] (Hilsdorf and Brameshuber, 1991)and Eq. [4-3] (Zhou et al., 1995).

$l_{ch} = 600(f_c')^{-0.3}\ (mm)$ Eq. [4-2]

$l_{ch} = -3.84f_c'+580\ (mm)$ Eq. [4-3]

Table 4-2, shows a comparison between chractristic length, based on the fracture energy values in Eq. [4-1], and avilable models, Eq. [4-2] and [4-3]. In general, it is understandable that the brittleness of concrete increases with the increase of compressive strength. Available models, Eq. [4-2] and[4-3] follow that observation. The models available do not accurtly predict the chractristic length of concrete when compared to values derived from experimentaly meassured the fracture energy, Eq. [4-1]. The previously derived models, Eq. [4-2] and [4-3] underestimate the value of the charactristic length for concrete with high compressive strength. In addition, for a high compressive strength, Eq. [4-3] yields negative values compromising its effectivness. Needless to say, UHPFRC does not follow the behaviour of conventional concrete. The significantly increased strength suggest a very brittle behaviour, however the addition of the fibre matrix results in otherwise a very ductile response. Consequenlty, resulting in inaccurate l_{ch} values. This behaviour is also demenostrated in the fracture behaviour of the test beams, Figure 4-3. Typically, in conventional concrete with no reinforcement, a crack results in a sudden failure. However, in UHPFRC, as shown in Figure 4-3, the test beam remian intact even after crack propogation to the surface. Therefore it is recomended to meassure the fracture energy experimentaly and to the calculate the charactaristic length from Eq.[4-1]. The charactristic legth is typically used in analysis involving shear design of larger members, beams or slabs, which are infulenced by the size effet; depth greater than 300 mm.

Table 4-2 Characteristic Length of Concrete 40-165 MPa

f_c' (MPa)	l_{ch}, Eq. [4-1] (mm)	l_{ch}, Eq. [4-2] (mm)	l_{ch}, Eq. [4-3] (mm)
40	500	198.39	426.4
55	742	180.31	368.8
57.8	532	177.65	358.04
58.7	489	176.83	354.59
61	649	174.80	345.76
63	503	173.12	338.08
74	478	164.96	295.84
75	394	164.29	292.00
137	769	137.13	53.92
163	693	130.16	-45.92

[4.3]Tension Stiffening

[4.3.1] Results and Observation

Tensile stresses developed in any reinforced concrete structure can easily cause cracking. Cracking loads can be captured at the point where a change in stress-strain slope is noticed. Typically, a sudden jump in the strain measurements corresponds to the first internal crack which eventually propagates to the surface of the reinforced member. Member TS1 and TS2 were subjected to an axial load while the members' responses were being monitored. TS1 and TS2 showed surface cracks at 140 kN and 100 kN respectively with an average tensile stresses of 3.42 MPa. Generally, after cracking, the tensile stresses carried by the tension stiffening specimen should decrease. However, because the presence of the fibre reinforcement the maximum tensile stress carried by the concrete increased to an average of 4.67 MPa. It should be noted, the concrete tensile stresses developed did not reach the tensile strength of concrete (8-10 MPa) as the reinforcement bars reach yielding strains. Ideally the test should be conducted until complete concrete failure; however the test was stopped as the reinforcement bars yielded, to avoid any catastrophic failure of the specimen due to the rupture of the reinforcement. Figure 4-4 shows a complete summary of the test results.

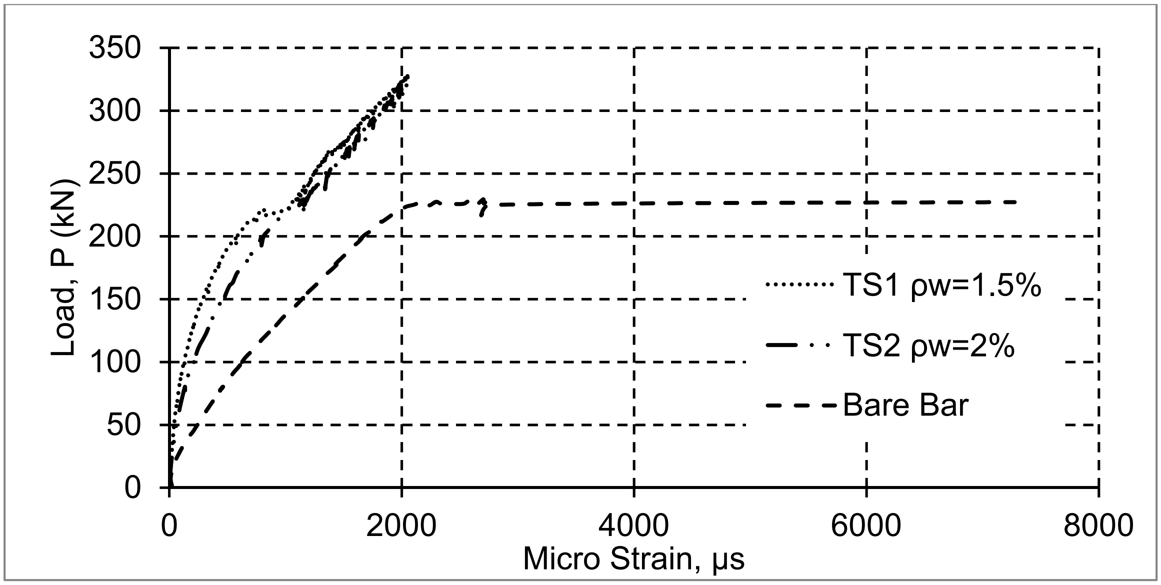

Figure 4-4 Average Load-Strain Response of Test Specimens Under Direct Tension

[4.3.2] Discussion of Results

Initially, the reinforced test specimen was assumed to have zero strain. Any axial deformation, Δ, due to the applied load, P, can be expressed as strain, ε_t, which is given by $\varepsilon_t = \Delta/L$, where L is the original length of the specimen. Typically, the reinforcement bar and the concrete section are assumed to be perfectly bonded. To maintain equilibrium the change in length in both the reinforcement bar and the concrete section is identical. Hence, the load applied, P, prior to cracking is taken partially by the concrete and the steel bar in accordance to the stiffness of the concrete and reinforcement bar. The average tensile stresses of concrete, f_t, shown in Figure 4-5, were calculated at each loading stage using equilibrium, Eq. [4-4].

$$f_t = [P - E_s A_s \varepsilon_s] / A_c \qquad \text{[Eq.4-4]}$$

Where, P: the applied load, E_s: the modules of elasticity of steel, A_s: the area of steel and ε_s: the strain in steel and A_c is the area of concrete.

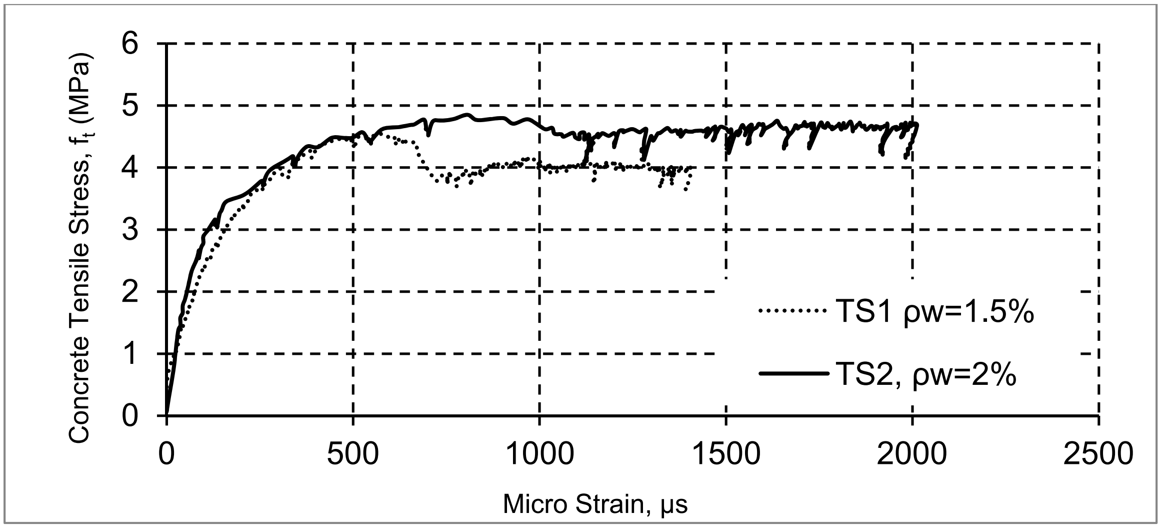

Figure 4-5 Average Concrete Stress in Test Specimen

The first transverse crack occurred, as expected, in the middle of the test specimens TS1 and TS2 at 140 kN and 100 kN, respectively, with an average tensile stresses of 3.42 MPa. The cracking tensile strength correlates accurately with the first significant change in the stress strain relation shown in Figure 4-5. It should be noted that the ultimate tensile strength of the UHPFRC used ranges from 8-10 MPa. Although the section first cracked at 3.42 MPa the concrete continued to take additional stresses due to the presence of the fiber reinforcement.

The results presented in Figure 4-4, where the difference between the load carried by the member and the load carried by the bare bar represents the tension stiffening behaviour of UHPFRC. Comparing those results to those of Fischer and Li (2002) several observations can be made. Fischer and Li (2002) compared the tension stiffening response of normal concrete and Engineered Cementations Composites (ECC), presented in Figure 4-6. The ECC used, is a type of concrete which utilized 1.5% by volume of polyethylene fibers, cement, fine aggregate (average grain size 0.3 mm), water, high-range water-reducing admixture. The ECC used had an ultimate tensile strength of 6.5 MPa and a compressive strength of 80 MPa.

Prior to the formation of cracks, all specimens had a similar response. The difference in the behaviour of the reinforced member and the bare bar is considered to be the effect of the tension stiffening of the uncracked section. After cracking, the comparison of the load-strain response shows a more significant contribution of UHPFRC when compared to ECC. Normal concrete showed the least tension stiffening contribution after cracking. Considering the tensile strength of all types of concrete, the significant contribution of UHPHRC and ECC is due to the load carried by the fiber matrix integrated within the mix. Prior to reaching the cracking strength, the load applied to the member is shared between the concrete and the steel bar based on their stiffness and volume fraction. Since the normal concrete section is not able to transfer loads after cracking; majority of the load is transferred and carried entirely by the steel bar by means of bond action. Typically in normal or high strength concrete after the formation of the first crack, a significant increase in the deformation is noticed. Subsequent to the transverse cracks, stresses accumulate causing longitudinal cracks, which eventually form more transverse cracks (Abrishami and Mitchell, 1997 ; Fischer and Li, 2002).

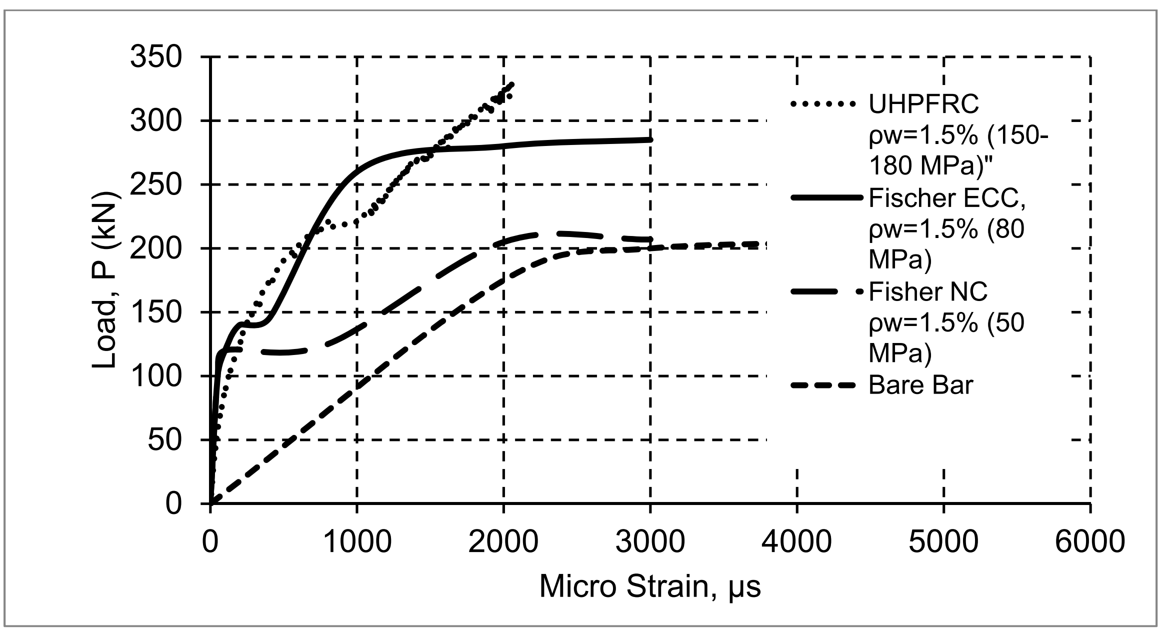

Figure 4-6 Load-Strain Relation of the Tension Stiffening Response of ECC and Normal Concrete (Fischer and Li, 2002)

The presence of fiber reinforcement has a distinct effect on the cracking response of the test specimen. When using UHPFRC the significant jump in the deformation was not noticed. This noted behaviour is characterized by the presence of steel fibers; which tend to tightly hold the cracks. It appears that such property increase the tension stiffening effect. After the propagation of the first crack, the stiffness of the concrete section remained relatively high to accommodate further elongation due to the applied load, creating additional transverse cracks propagated symmetrically along the length of the test specimens, as presented in Figure 4-7. This behaviour is due to the fiber bridging action, which transfers stresses between two cracked sections rather than transferring the load to the steel bar. In addition the yielding force of the embedded bar was 315 and 300 kN for TS1 and TS2 respectively, while the yielding force of the bare bar was approximately 215 kN. This behaviour is rather comparable to previous work for tension stiffening of fiber reinforced concrete. Pervious work concluded in a non fiber reinforced concrete tension stiffening model, the yielding force of the bare bar and the embedded bar is the very close to one another (Abrishami and Mitchell, 1997 ; Fischer and Li, 2002 ; Dawood and Marzouk, 2012).

Table 4-3 Cracking Behaviour of Tension Stiffening Test Specimen

Specimen Name	f'c (MPa)	Number of Cracks	Elongation (mm)	Average Crack Width (mm)
TS1	159.8	17	2.22	0.13
TS2	157.5	19	3.22	0.17

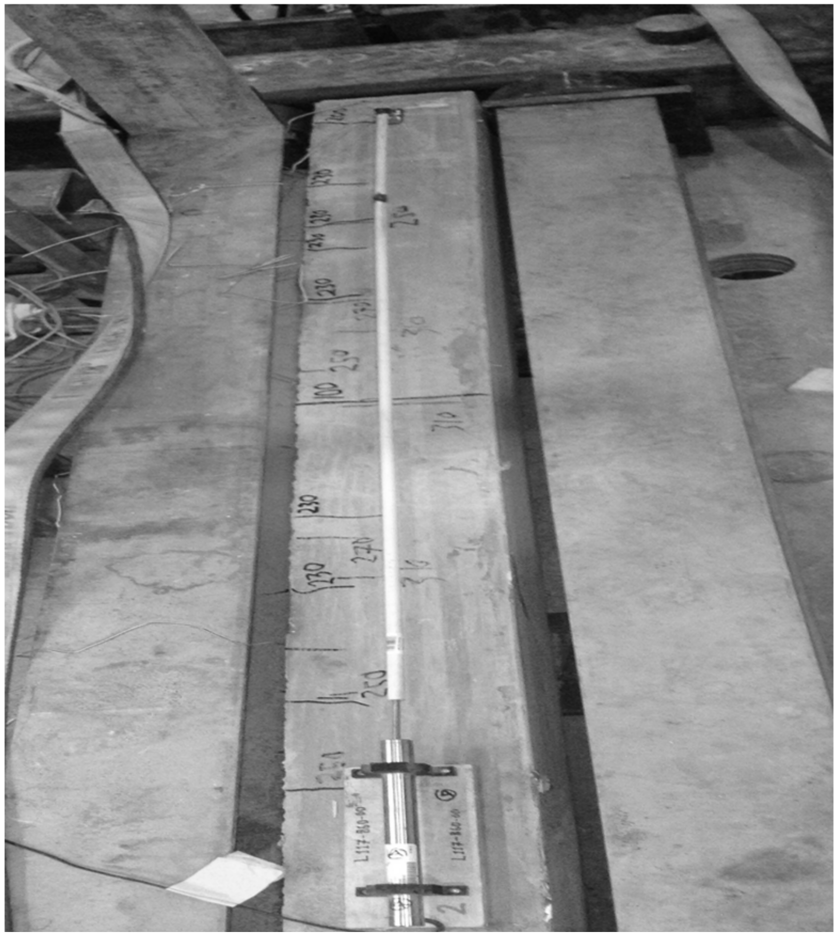

Figure 4-7 Typical Cracking Pattern of Tension Stiffening Test Specimen, TS2

[4.3.3] Comparison to Previous work

There hasn't been much development in the area of tension stiffening of UHPFRC. However, the basic principles of previous models can be applied. In 1995, Chen and Marzouk developed a tension stiffening model to predict the behaviour of high strength and normal strength concrete represented. They developed two equations representing the ascending and the descending portions of the tension stiffening behaviour. For the purposes of comparison only the ascending model will be used represented by Eq [4-5]

$$f_t/f_t' = 2\varepsilon_t/\varepsilon_p - (\varepsilon_t/\varepsilon_p)^2 \quad \text{[Eq. 4-5]}$$

Where, ft : the tensile strength of concrete, ft' : the peak tensile strength of concrete, *εt:* tensile strain of concrete, *εt'* : tensile strain of concrete at peak strength. Since the model does not incorporate fiber reinforcement, a few assumptions have to be made. Typically, the peak tensile strength is associated with the cracking strength of concrete. Considering Eq. [4-5], the peak tensile strength can be replaced with the cracking strength of UHPFRC.

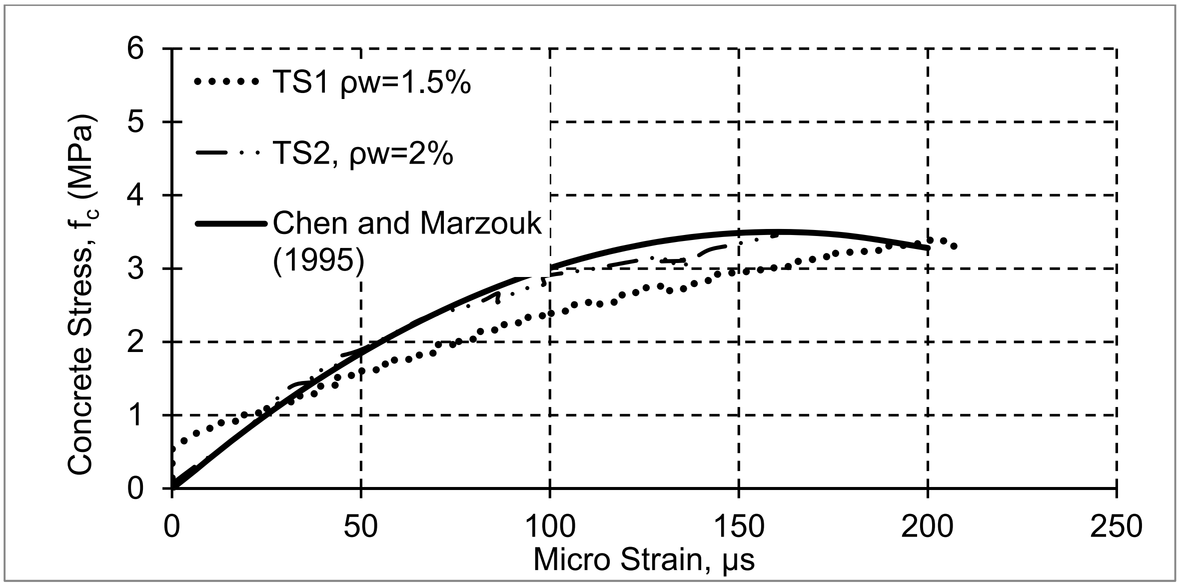

Figure 4-8 Comparison of Tension Stiffening Model

As shown in Figure 4-8, there is a strong correlation between the uncracked section of UHPFRC and the Eq. [4-5]. Such behaviour, suggest that UHPFRC behaves very similar to non fiber reinforced concrete. However to fully understand the tension stiffening behaviour of UHPFRC further investigation is required.

[4.4]Shear Friction Strength

[4.4.1] Results and Observations

The following results are based on the parameters measured during the push-off test specimens detailed in Chapter 3. There parameters include the shear load ,V, the shear displacement parallel to the shear zone , Δ, and maximum steel strain are summarized in Table 4-4. Test Specimen SF1, failed at an ultimate load of 445 kN and a maximum layer slip of 2.3 mm. test specimen SF2 and SF3 failed at an ultimate load of 524 kN and 530 kN respectively with layer slip of 3.6 mm and 1.5 mm respectively. In addition the load-slip curves and the load-steel strain curves are presented in Figure 4-9.

Table 4-4 Test Results of Push-Off Specimens

Specimen Name	Shear Area (mm^2)	Steel Ratio ρ_v (%)	Cracking load V_{cr} (kN)	Ultimate load V_u (kN)	Maximum Displacement Δ_{max} (mm)
SF1		0	400	445	2.3
SF2	305x101.5	0.5	N/A	524	3.6
SF3		1	N/A	530	1.5

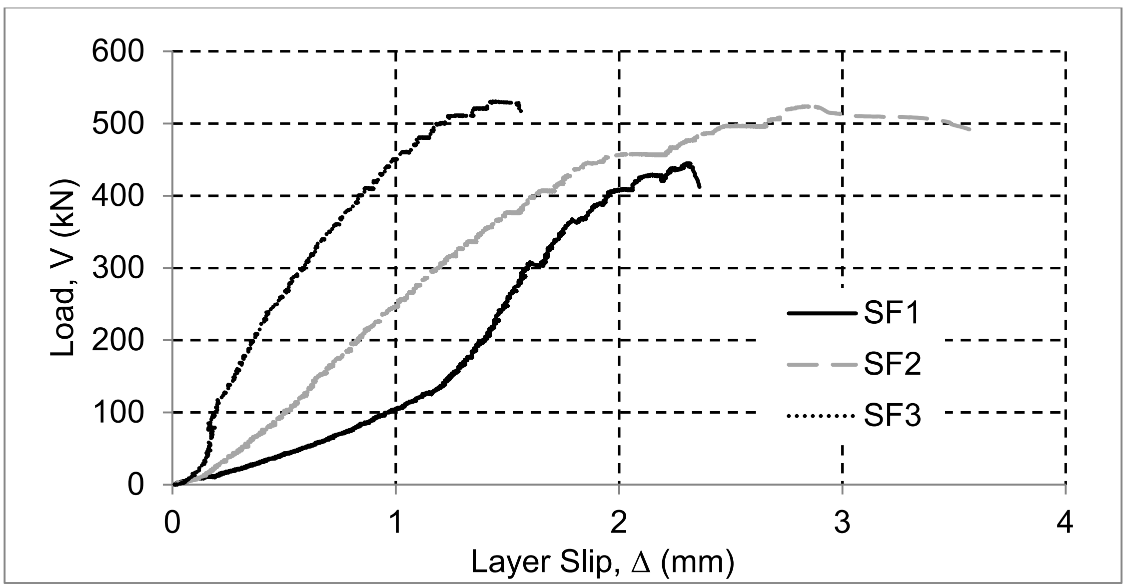

Figure 4-9 Load-Slip Relation of Push-Off Test Specimens

[4.4.2] Analysis and Discussion of Results

[4.4.2.1] Effect of Reinforcement ratio on Carrying Capacity

In the control test specimen, SF1 ($\rho_v = 0$), one surface crack was observed at a load of 400 kN approximately 90% of the ultimate load 445 kN, as shown in Figure 4-11 (a). The crack was initiated along the critical shear friction plane spanning along the entire length of the shear zone as shown in Figure 4-10 (a). Referring to Figure 4-9, it is observed at 125 kN a change in the slope of the load-slip curve; indicating internal cracking far beyond ultimate failure. Such behaviour, internal cracking, is consistent with UHPFRC. Both SF2 and SF3 (ρ_v= 0.5 and ρ_v= 1 respectively) didn't show shear cracking at all, due to the significant contribution of the transverse reinforcement. However, both SF2 and SF3 showed significant cracking at the support and load application where flexural stresses developed due to the nature of the setup.

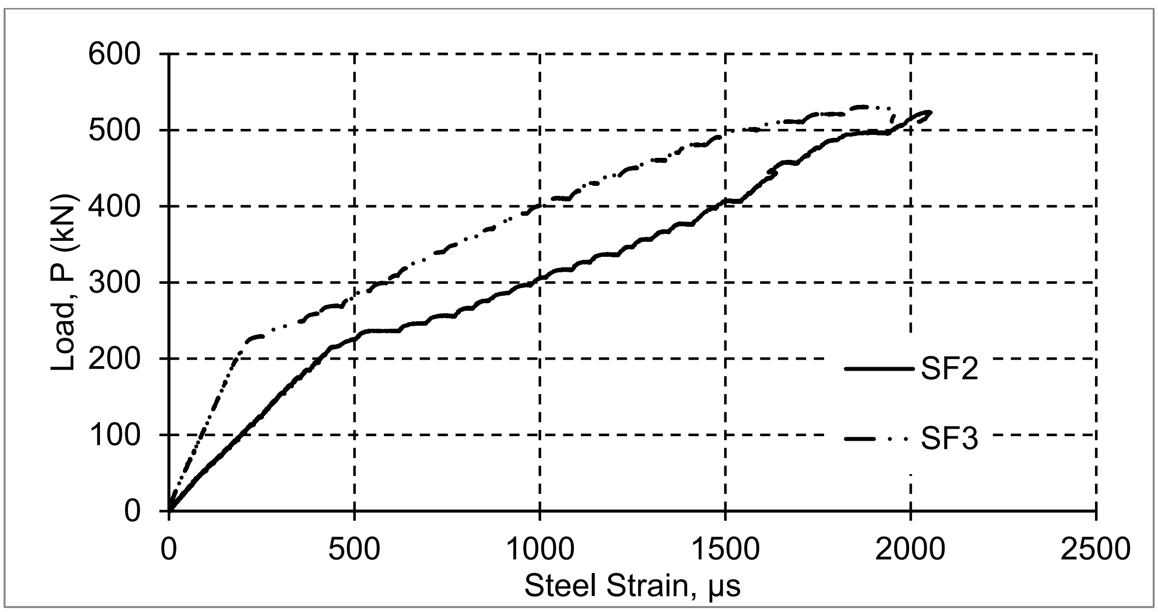

Figure 4-10 Load-Transverse Steel Strain of Push-Off Test Specimens

Taking a closer look at the results it observed, that the steel reinforcement in fact yielded, as shown in Figure 4-10. Furthermore, at approximately 210 kN and 230 kN a significant change in the slope of the load-strain response of SF2 and SF3 respectively is noticed; indicating internal cracking. Comparing the internal cracking load of SF1 SF2 and SF3, it is apparent the introduction of the shear reinforcement increased the cracking load of the concrete section. Such behaviour is referred to as confinement action in which the introduction of shear reinforcement enhanced the quality of concrete.

From Figure 4-9, it can be seen that there is a significant variability between the shear displacements of the test specimens. At the early stage of the specimen response, load-slip, a significant increase in the stiffness of the response is noted. For instance, the stage Δ=1mm, the significant increase in the stiffness response is illustrated by the increased corresponding load, 104 kN , 246 kN and 450 kN for SF1, SF2 and SF3 respectively.

Figure 4-11 Cracking behaviour of Push-Off Test Specimens (a) SF1, (b) SF2 and (c) SF3

[4.4.3] Shear Friction Strength of Concrete

The relation between the ultimate shear load, V_u, and the interface steel reinforcement is shown is Figure 4-10. For comparison purposes, previous experimental data from shear friction test conducted by Khan and Mitchell (2002) represented by Eq. [4-6] is taken into consideration. This particular set of results was chosen as it provides experimental results for concrete with a wide range of compressive strength 27-124 MPa. In addition the design guideline, Eq. [4-6], included not only results from the experiment conducted by Khan and Mitchell (2002), but a wide variety of experimental results conducted by Anderson (1960) and Mattock et al. (1969) on normal strength concrete. The design guideline was developed to give a simple and accurate prediction of the shear friction capacity of normal, high strength concrete. The equation incorporates a frictional value (μ=1.4) and a component for bond and asperity shear ($0.5f'_c$). Khan and Mitchell (2002) concluded by taking the component for bond and asperity shear as a percentage of the compressive strength, the equation better predicted results for normal and high strength concrete. An upper limit was set at 20% of the compressive strength as it agreed with khan and Mitchel (2002) results and ACI 318-08. The result of khan and Mitchell (2002) are represented by Eq. [4-6].

$$v_u = 0.05\, f'_c + 1.4\, \rho_v f_y \leq 0.2\, f'_c \qquad \text{[Eq. 4-6]}$$

Though, test specimen SF2 and SF3 did not entirely fail in the shear critical zone as seen in Figure 4-10, the interface steel reinforcement did in fact yield as shown in Figure 4-11. Such behaviour can be characterized as failure. Following the same approach as Khan and Mitchell (2002), the test results of the UHPFRC Push-Off experiment can be compared to specimens of similar geometric dimension. The results of the test conducted seem to follow the same behaviour as reported by previous researchers (Anderson, 1960; Mattock et al., 1969 Khan and Mitchell, 2002). Figure 4-12 illustrates the results of the UHPFRC test in comparison to the normal and high strength concrete as well as the Eq. [4-5]. The ACI provision tends to give very conservative results when compared with existing data, ignoring entirely the bond and asperity shear component as reported by Khan and Mitchel (2002) as seen in Figure 4-12. However, the model proposed by Khan and Mitchel (2002) can still provide a good agreement with the experimental test results with UHPFRC presented in this study.

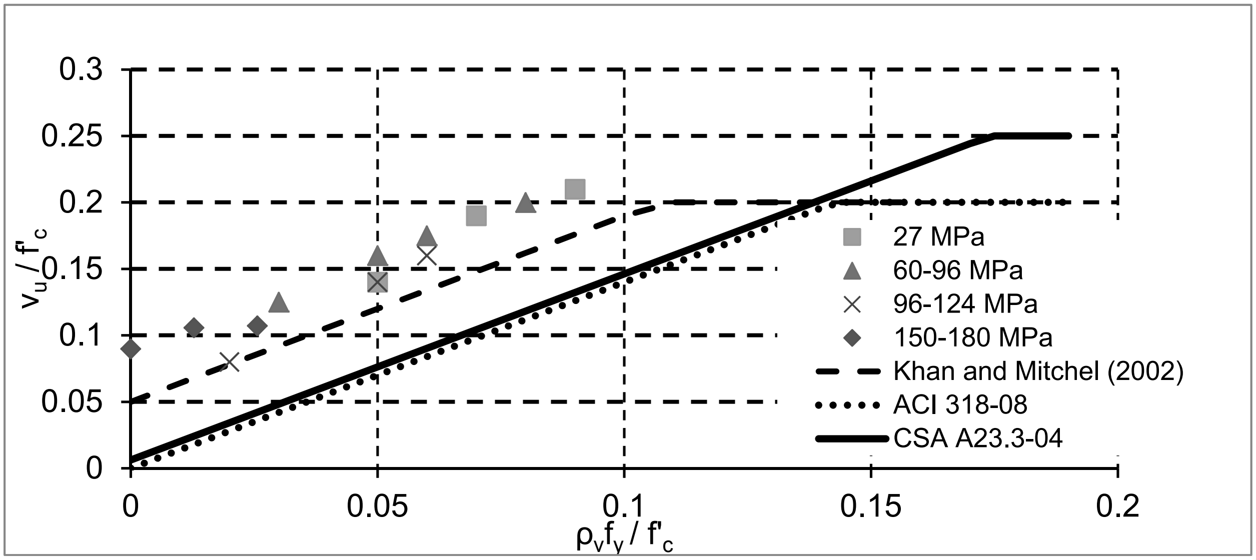

Figure 4-12 Comparison of Push-Off Specimens Test results

[4.4.4] Fiber Effect on Shear Friction Strength of Concrete

As proposed by many researchers, (Aoude et al. , 2012; Japan Concrete Institute Standard, 2003; Kwak et al., 2002 and Naraynan and Darwish, 1987), the behaviour of fiber reinforced concrete is better represented by investegating the fiber effect. A concept relating design guidelines directly to the fiber present in the concrete mix. Such concept, can be directly applied to shear friction behaviour.

Another way to look at the shear friction capacity of UHPFRC beams is to study the fiber contribution effect rather than the property of the material as a whole. Considering a UHPFRC shear friction zone without any additional steel reinforcement, the steel fibers are assumed to be evenly distributed along the cross section; it can be considered, hypothetically, the steel fibers acting as transverse reinforcement bars along the shear zone. Based of the cross sectional area of the shear zone and on the steel fiber content of the mix, the area of the steel reinforcement, A_f,can be calculated. The area of the steel fibers should be corrected to account for fiber distribution. This correction factor, $\alpha = 3/8$ (Aoude et al. 2012), accounts for the random orientation of the fibers crossing any arbitrary cracking plane. In addition a correction factor, $\eta_1 = 1/2$ (Aoude et al. 2012), which accounts for the embedment length across the cracking plane is considered.

The factor η_1 was developed for steel fibers that are 0.55 mm in diameter and 30 mm long. The steel fibers used in the present study are 0.2 mm in diameter and 12 mm long. Taking that into consideration, η_1 can be significantly reduced to accommodate the reduction in fiber length. In addition the pullout strength of the steel fibers is based not only on the embedment length but also on the area of each individual fiber. Considering the area and the length of each individual fiber, $\eta_1=1/2$ can be modified to $\eta_2 = 1/8$. Considering both factors the hypothetical steel fiber area can be modified to an effective steel fiber area where $A_{eff} = \eta_2\ \alpha\ A$. Further details are described in [5.1.3.2]. Considring this theory, Eq. [4-6] can be modified to incorprate the effect of fibers. The resulting propossed expression presented by Eq.[4-7] tends to follow the same accuracy as originally proposed by Khan and Mitchel (2002). Results of the comparrison is summarized in Figure 4-13 and Table 4-5, as seen the proposed equation, Eq. [4-7], predicts the shear friction stress wit great accuracy, where the average ratio between the experimental results and the predicted values based on Eq. [4-7] was 1.09.

$$v_u = 0.05\ f'_c + 1.4\ [\rho_v f_y + \alpha\eta_2\rho_f f_{fy}] \leq 0.2\ f'_c \qquad \text{[Eq. 4-7]}$$

Where, v_u: ultimate shear stress capacity, f'_c: concrete compressive strength, ρ_v: shear friction reinforcement ratio and f_y: yield stress of reinforcement bar, α: fiber orientation factor 3/8,

η_2: Embedment length factor 1/8, ρ_f: fiber reinforcement ratio f_{fy}: yeilding strength of fiber reinforcement.

Table 4-5 Comparison of Test Results with Existing Equation

Specimen Name	Exp (kN)	ACI (kN)	CSA (kN)	Eq. [4-6] (kN)	Proposed (kN)
SF1	445	0	30.96	247.66	373.62
SF2	524	86.68	117.64	334.34	460.3
SF3	530	137.36	204.32	421.02	546.98
Average Exp/Eq		3.03	7.14	1.54	1.09
STDEV Exp/Eq		3.02	6.33	0.26	0.11
COV Exp/Eq		0.99	0.88	0.17	0.10

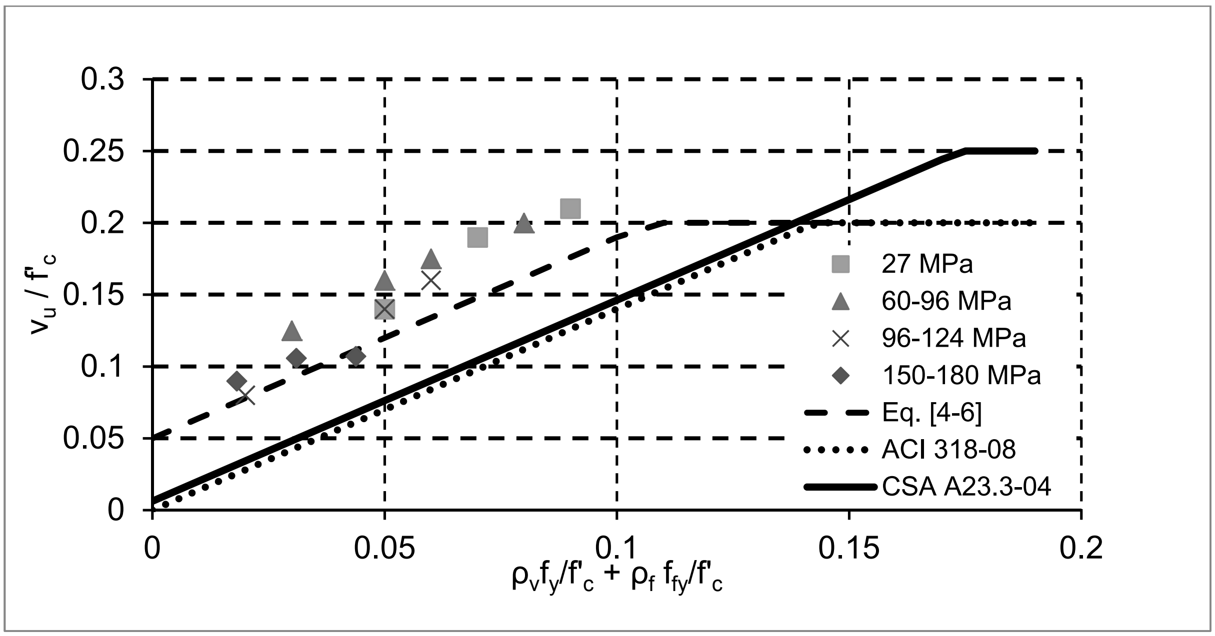

Figure 4-13 Comparison of Test Results Considering Fiber Effect based on Eq. [4-6]

Chapter [5]

Analysis of Structural Beam Behaviour

[5.1] Flexural and Shear Behaviour of UHPFRC Beams

[5.1.1] Results and Observations

In all the beams tested the maximum load was obtained far after yielding of reinforcement bars. Test beams were considered "failed" when it was no longer possible to apply load. Table 5-1 and Figure 5-1 summarize the results of the tests, with the deflection measurements at center span. In all tested beams flexural cracks were mainly observed within the pure bending region. In addition beam SB4, ρ_w= 2.5%, flexural cracks where observed outside the pure bending region which eventually curved towards the loading points forming flexure-shear cracks. These cracks, commonly, would result in sudden failure under normal circumstance, lack or shear reinforcement and brittleness of concrete. However, the sudden catastrophic shear failure is prevented in this case due to the presence of the fiber matrix, which held the cracks preventing them from suddenly propagating. The effect of the fiber reinforcement is undoubtedly significant in the analysis of UHPFRC structural members. The fiber reinforcement appears to considerably enhance the capacity of the concrete beams in terms of shear and flexural capacity by sealing formed cracks.

Table 5-1 Test Results of UHPFRC Beams

Beam Name	f'c (MPa)	Experimental Load, P (kN)	Maximum Deflection (mm)	Maximum Steel Strain (μs)
SB1	168.15	90	11.46	N/A
SB2	145.14	235	17.5	3532
SB3	160.38	113	36.05	3051
SB4	167.08	330	19.02	3280
SB5	172.08	169	45.05	3597

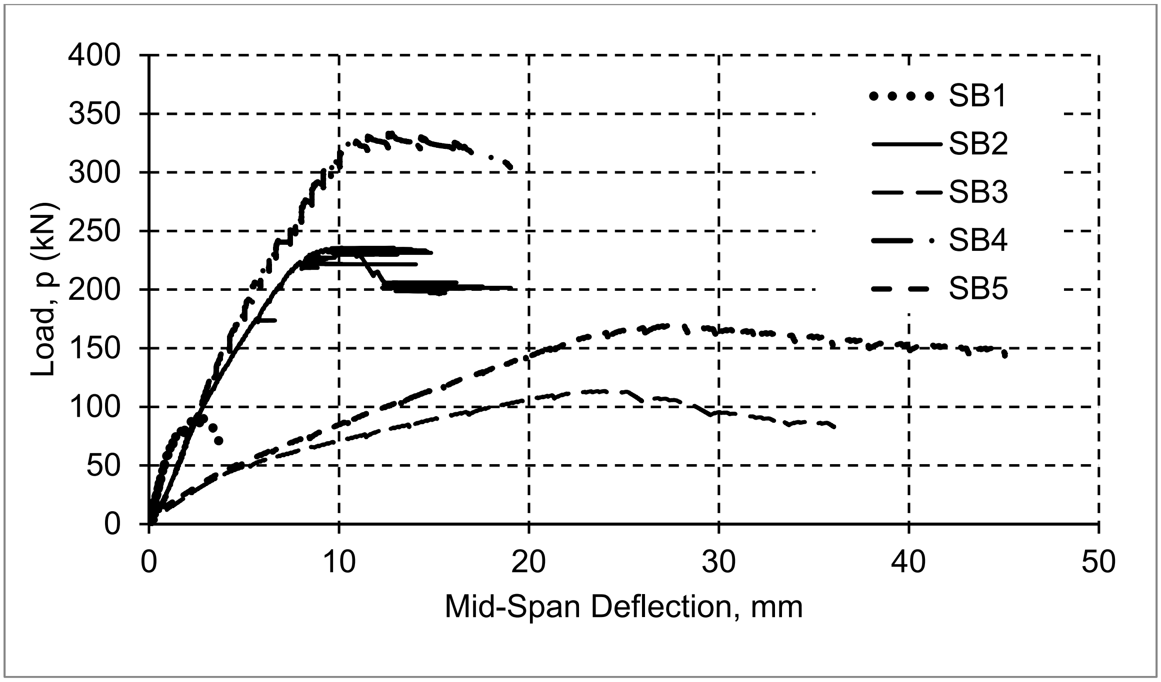

Figure 5-1 Comparison of UHPFRC Beams Response

[5.1.2] Effect of Reinforcement Ratio

Ultimately, all beams failed in a flexural manner, with only SB4 showing evidence of shear cracks. SB1, SB2 and SB4, all have the same cross sectional area and span, while the reinforcement ratio was 0%, 1.25% and 2.5% respectively. SB1 failed at an ultimate load of 90 kN with a maximum mid-span deflection of 11.46 mm. The introduction of steel bars as means of reinforcement significantly increases the ultimate load carrying capacity and the maximum mid-span deflection. SB2 had an ultimate capacity of 235 kN and a maximum deflection of 17.5 mm. While SB4 had an ultimate capacity of 330 kN and a maximum deflection of 19.02 mm. the maximum mid-span deflection appears to slightly increase with the introduction of steel reinforcement; a phenomena expected of reinforced concrete beams. Additionally, it was observed that for beams as the reinforcement ratio doubled the ultimate load capacity were increased by 30%. However the total deflection was increased by 8% and 20% for beams with a/d = 2.33 and 4.66 respectively.

The steel fiber reinforcement has a distinct effect on the cracking behaviour of the UHPFRC beams. SB1, showed one crack at the mid-span. However, with the introduction of the steel bars a significant improvement in the structural response was noted. SB2 showed a higher number of cracks, at the constant moment region, than SB1. While, SB4 showed the highest number of cracks within the constant moment location. In general steel bar reinforcement tends to help in cracking control, with the addition of the steel fiber it seems that the cracks are significantly controlled. The cracking pattern of SB1, SB2 and SB4 is shown in Figure 5-2.

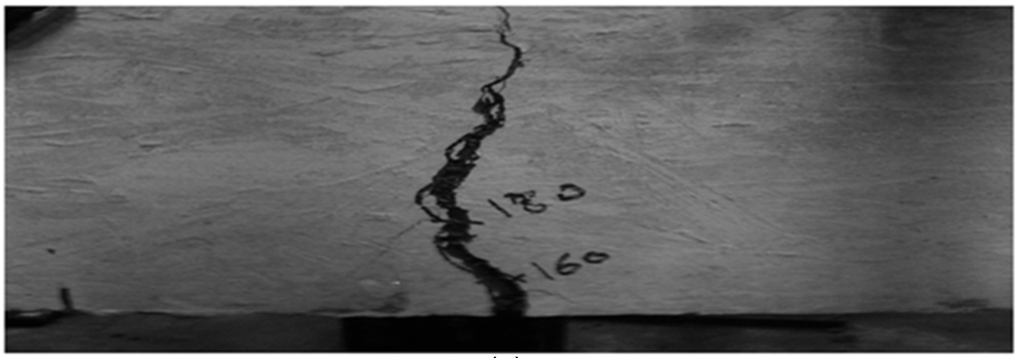

(a)

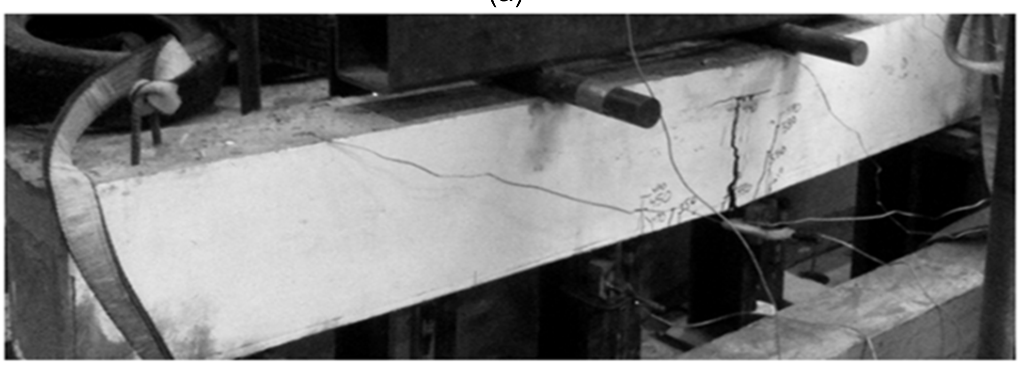

(b)

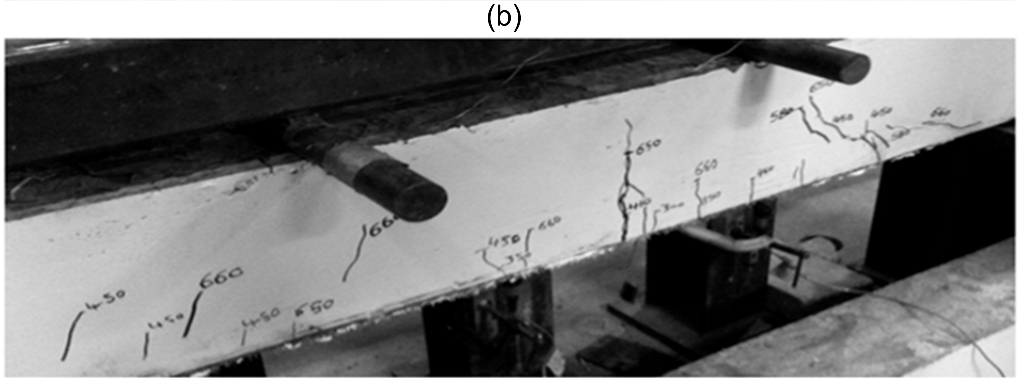

(c)

Figure 5-2 Cracking Behavior of UHPFRC Beams; (a) SB1, (b) SB2 and (c) SB4

[5.1.3] Flexural Behaviour

In general, reinforced concrete beams undergo four distinct stages of flexural behavior; elastic uncracked, elastic cracked, yielding and failure. It is assumed that during the elastic cracked stage, flexural stresses are no longer carried by the concrete but rather by the reinforcement bars (Brzev and Pao, 2006). While this assumption holds true for concrete made with no fiber reinforcement, the experimental, beams made with UHPFRC, results suggest otherwise.

[5.1.3.1] Concrete Contribution as a Material Property

The load-Deflection, at center span, relation of beams SB1, SB2, SB3, SB4 and SB5 is presented in Figure 5-1. It's also observed that all the beams tested exceeded the yielding strain of steel (0.002). This behavior is a prime indicator that the fibers have significant contribution to improve the capacity of the reinforced beams after the yielding of steel. Considering the basic principles of equilibrium forces acting on a rectangular cross section, where the internal bending moment is resisted by a force couple, T_r and C_r (Brzev and Pao, 2006). Using the compatibility principle, $T_r=C_r$, the resistance moment due to steel reinforcement, can be calculated as per Eq. [5-1]. The mentioned basic principle is the basis for flexural design equation found in Canadian concrete design code CSA A23.3-04.

$$M_r = T_r\,(d-a/2) \qquad \text{[Eq.5-1]}$$

The effect of fiber is clearly demonstrated in the test results summarized in Table 5-2. The ultimate load capacity is much greater than the load required to cause a maximum steel strain (yielding strain) of 0.002, indicating once more the test specimens carry tensile stresses beyond yielding stage, due to the fiber reinforcement. Eq. [5-1] can then be modified to account for the additional flexural stresses carried by the fiber reinforced concrete. The proposed model, Eq. [4-6] includes the flexural stresses carried by the fiber reinforcement, as observed during the experiment. As it can be seen in Table 5-2, the proposed model predicts the flexural capacity of UHPFRC with better accuracy. Figure 3, demonstrates a correlation between the experimental results and the predicted values based on the proposed model.

$M_r = T_r\ (d\text{-}a/2) + (f_r\ I)\ /\ y_t$ [Eq.5-2]

Where,

f_r: Modulus of Rupture, determined experimentally from SB1, I: Moment of Inertia and y_t: distance from the extreme tension fiber to the centroid of the beam

Table 5-2 Comparison of Flexural Strength and Proposed Eq. [5-2]

Beam Name	Exp (kN)	CSA (kN)	CSA /Exp	Proposed Eq. [5-2] Steel Capacity (kN)	Proposed Eq. [5-2] Concrete Capacity(kN)	Proposed Eq. [5-2] Total (kN)	Eq. [5-2]/Exp
SB1	90.5	90.48	0.99	N/A	90.48	90.48	1.00
SB2	235.5	101.53	0.43	101.53	90.48	192.01	0.82
SB3	113.5	50.89	0.44	50.89	45.24	96.13	0.85
SB4	330.5	199.04	0.60	199.04	90.48	289.53	0.88
SB5	169	99.66	0.58	99.66	45.24	144.90	0.86
			Avg = 0.61 STDV = 0.2 COV = 0.33				Avg = 0.88 STDV = 0.07 COV = 0.08

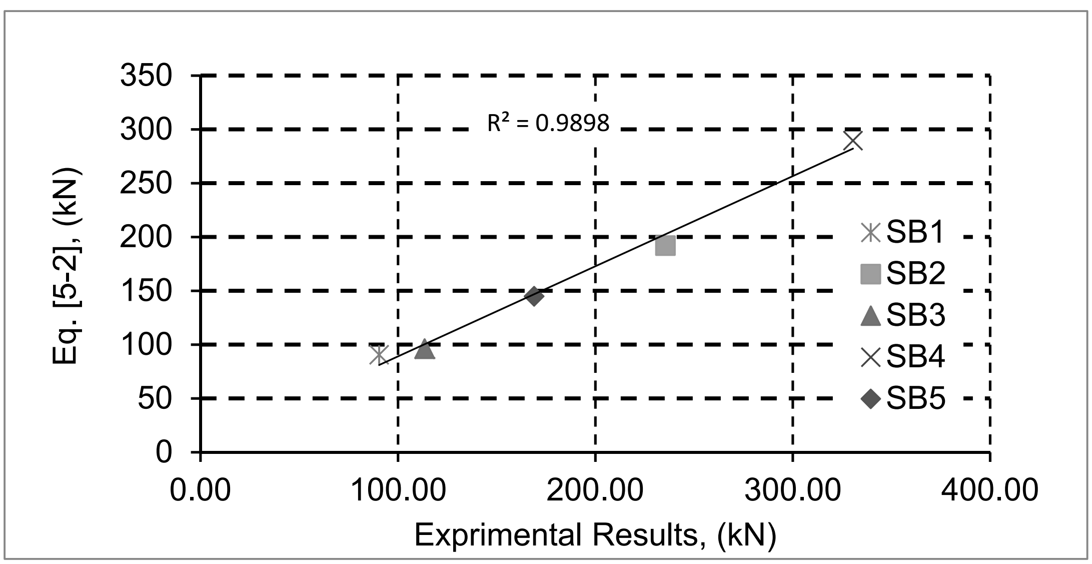

Figure 5-3 Comparison of Test Results and Proposed Equation Eq. [5-2]

[5.1.3.2] Concrete Contribution as Fiber Content

Another way to look at the flexural capacity of UHPFRC beams is to study the fiber contribution effect rather than the property of the material as a whole. Considering a UHPFRC beam without any additional steel reinforcement Figure 5-4 (a) subjected to four point loading; the steel fibers are assumed to be evenly distributed along the cross section. Considering, hypothetically, the steel fibers as two reinforcement bars as shown in based of the cross sectional area of the beam of the steel fiber content of the mix, A_f, where D is the depth of the beam, b is the width of the beam and V_f is the fiber content, Figure 5- 4(b). The area of the steel fibers should be corrected to account for fiber distribution. This correction factor, $\alpha = 3/8$ (Aoude et al. 2012), accounts for the random orientation of the fibers crossing any arbitrary cracking plane. In addition a correction factor, $\eta_1 = 1/2$ (Aoude et al. 2012), which accounts for the embedment length across the cracking plane is considered.

The factor η_1 was developed for steel fibers that are 0.55 mm in diameter and 30 mm long. The steel fibers used in the present study are 0.2 mm in diameter and 12 mm long. Taking that into consideration, η_1 can be significantly reduced to accommodate the reduction in fiber length. In addition the pullout strength of the steel fibers is based not only on the embedment length but also on the area of each individual fiber. Considering the area and the length of each individual fiber, $\eta_1=1/2$ can be modified to $\eta_2 = 1/8$. Considering both factors the hypothetical steel fiber area can be modified to an effective steel fiber area, A_{eff}, Figure 5-4(c).

Based on previous work (Federal Highway Administration, 2006), the maximum compression strain of UHPFRC was determined to be approximately 3500με. Since the ultimate strain in compression of UHPFRC is the same as normal concrete; the basic assumptions can be made as specified by the CSA A23.3-04 for flexural capacity of reinforced concrete beams. The UHPFRC beam can now be considered as beams having two distinct types of reinforcement.

The resultant flexural capacity can be estimated according to Eq [5-3]. All parameters in Eq. [5-3] are calculated in accordance to CSA A23.3-04

$$Mr = M_s + M_f \qquad \text{[Eq.5-3]}$$

Where,

$M_s = T_{rs}\ (d-a/2)$, based on traditional steel reinforcement

$M_r = T_{rf}\ (d-a/2)$, based on steel fibers reinforcement

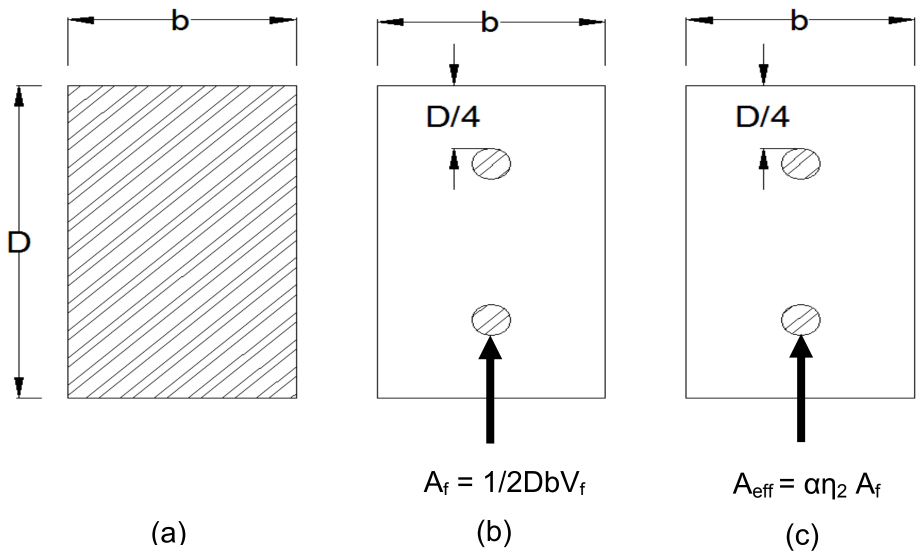

Figure 5-4 Steel Fiber Distribution in UHPFRC

Table 5-3 Comparison of Flexural Strength and Proposed Eq. [5-3]

Beam name	Exp (kN)	CSA (kN)	CSA/Exp (kN)	Proposed Eq. [5-3] Steel Capacity (kN)	Proposed Eq. [5-3] Fiber Capacity (kN)	Proposed Eq. [5-3] Total (kN)	Eq. [5-3]/Exp
SB1	90.5	90.48	0.99	N/A	99.15	99.15	1.10
SB2	235.5	101.53	0.43	101.53	98.98	200.52	0.85
SB3	113.5	50.89	0.44	50.89	49.55	100.44	0.89
SB4	330.5	199.04	0.60	199.04	99.14	298.19	0.90
SB5	169	99.66	0.58	99.66	49.58	149.24	0.88
			Avg = 0.61				Avg = 0.92
			STDV = 0.2				STDV = 0.1
			COV = 0.33				COV = 0.1

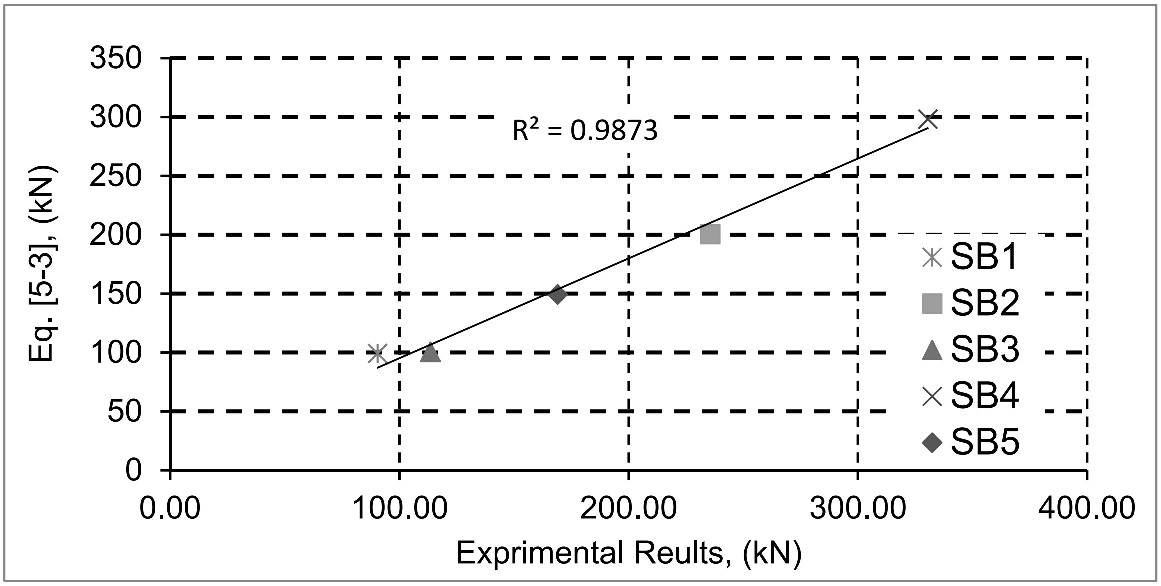

Figure 5-5 Comparison of Test Results and Proposed Equation Eq. [5-3]

As seen in Figure 5-5 and Table 5-3, the use of fiber effective area yields rather accurate results. Eq. [4-7] as mentioned ignores the effect of concrete properties and focuses only on the fiber content as means of the effective fiber bar. To further explain, the proposed Eq. [5-1] provides adequate prediction based solely on the fiber content. Generally, UHPFRC utilizes 2%, assuming a different percentage of fiber reinforcement Eq. [5-1] will maintain its accuracy.

[5.1.3.3] Moment Curvature

The results of the experimental program are compared to the theoretical moment curvature behaviour of the beam based on basin principle and equilibrium properties. The flexural behaviour estimated, is based on the equilibrium of forces and strain compatibility. The behaviour estimated follows the following assumptions:

- The stress-strain relation of UHPFRC in compression is assumed to be linear for the ascending portion.

- When a moment is applied to a reinforced concrete beam, it is assumed that the strain in the compression zone is linear and parabolic in the tension zone
- The stress strain relation of the steel bars is assumed to be linear until yielding after which the relation is constant equal to the yielding strength of steel

Figure 5-6, compares the theoretical behaviour and the experimental behaviour of the test beams SB2 and SB3. The beams compared both had a reinforcement ratio of 1.25%. The theoretical model estimates a yielding moment of 136 MN.mm, while the experimental results showed a yielding moment of 114 MN.mm and 122 MN.mm for SB2 and SB3 respectively. The experimental results show a good comparison with the theoretical behaviour. The cracking moment predicted by the theoretical calculation is 29.85 MN.mm. the experimental cracking moment is 27.14 MN.mm and 32.94 MN.mm for SB2 and SB3 respectively. The experimental results once again suggest the contribution of concrete, due to the fibers, in the carrying capacity after cracking.

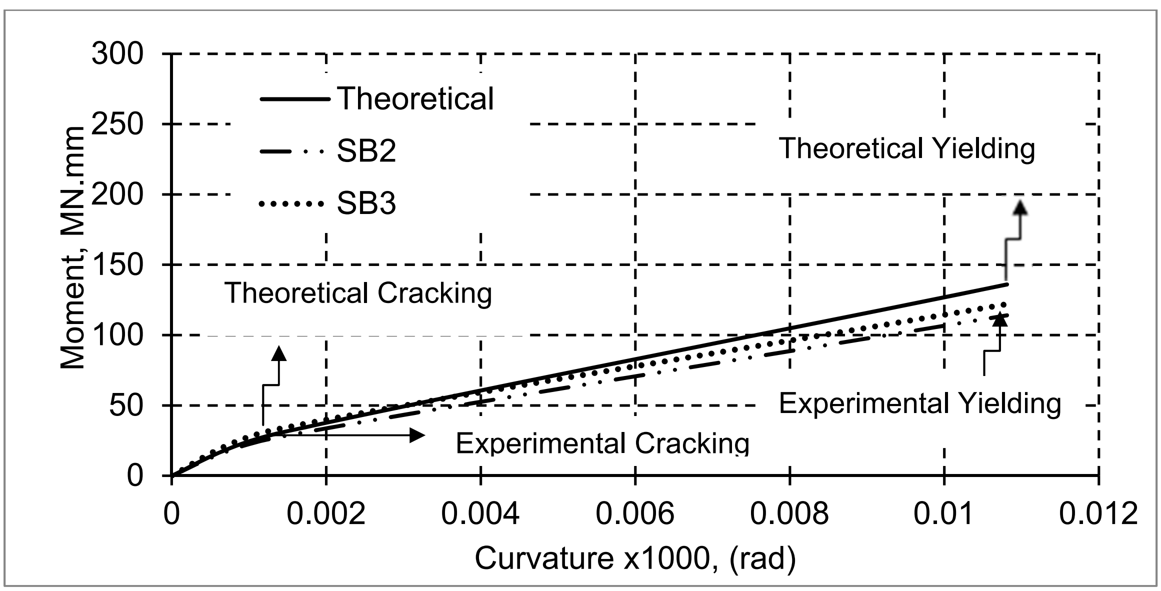

Figure 5-6 Moment Curvature behaviour of UHPFRC

[5.1.4] Shear Behaviour

Available design building codes such as CSA A23.3-04 and ACI 318-08 have simplified design guidelines for shear strength of beams without stirrups. In addition, various models have been developed to address the issues regarding shear strength design. All of the available design criteria are based on the assumption of the increased brittleness of concrete with increase in compressive strength. There have been many developments in design models for the use of fiber as a means of reinforcement. The majority of the models developed are based factors affecting shear strength such as: reinforcement ratio, shear span to depth ratio (a/d) and concrete strength. Nonetheless, these models were developed for the use of fiber as reinforcement for high strength concrete to reduce the brittleness of the material. There is yet to be a major development for such design equation for UHPFRC.

Table 5-4 Comparison of Shear strength of UHPFRC

Beam	CSA (kN)	ACI (kN)	Japan (kN)	Ashour (kN)	Kwak et al. (kN)	Narayanan et al. (kN)	Experimental (kN)
SB1	105.25	92.33	297.18	168.25	7.7533	286.11	90.5
SB2	97.79	85.78	303.71	160.90	381.99	297.65	235.5
SB3	102.79	90.17	303.93	84.07	100.38	112.42	113.5
SB4	104.92	92.03	305.92	174.99	526.94	378.67	330.5
SB5	106.48	93.40	306.01	88.62	131.09	127.27	169

While all test beams failed in flexure manner, certain conclusion can be drawn regarding the shear behaviour. As it can be seen above, Table 5-4, none of the North American design codes predict, with precision, the shear strength of UHPFRC as the experimental load far exceeded the shear capacity. It's mainly due to the lack of presence of the steel fiber effect in the available models. Many studies suggested the available North American codes do not safely consider parameters such as f_c', *a/d* and ρ_w with respect to shear strength of concrete members made with HSC and no stirrups. Models developed to address the issue regarding shear strength in concrete have, in the past, successfully done so. However, most of the proposed models for shear strength lack the effect of fiber reinforcement.

All of the tested beams showed a, considerably, high shear strength capacity compared to the available design codes. All beams ultimately failed in a ductile flexural failure. Looking at SB3, it's clear that the fiber reinforcement tripled the shear capacity, when compared with the recommended design equations by the CSA A23.3-04 and ACI 318-08. The effect of fiber reinforcement can be seen clearly in SB3, Figure 5-2 (c), where in fact shear cracks developed in the tension face propagating towards the loading point, ultimately failing in a flexural. Usually, due to the absence of stirrups, the concrete member will suddenly fail. However due the fiber matrix the crack was prevented of suddenly propagated and the beam ultimately failed in flexural manner.

Previously mentioned shear design equations (Ashour et al. , 1992; Kwak et al., 2002; Naraynan and Darwish, 1987), seem to, significantly, underestimate the shear capacity of beams having and a/d ratio of 4 while overestimating the shear capacity of beams with a low a/d ratio. As it can be seen from Table 5-4, SB 2 and SB4, are extremely underestimated when compared to the experimental results. Preliminary results indicate the Japanese UHPFRC design guidelines (Japan Concrete Institute Standard, 2003) tend to yield the most accurate results. The advantage of such models is the incorporation of the tensile strength in conjunction with fiber reinforcement ratio. It appears when dealing with UHPFRC the tensile strength and fiber reinforcement ratio is of a greater importance than the compressive.

Chapter [6]
Conclusion

[6.1]Summary

As a new material UHPFRC, proves to have superior qualities when compared to normal and high strength concrete. The development in the concrete's qualities is the product of the precisely optimized nano materials. In addition**,** the fiber matrix integrated within the concrete mix proves to effectively improve the post-cracking behavior of concrete. The introduction of fibre reinforcement proves to increase, significantly, the ductility of the concrete matrix; resulting in a concrete material that behaves rather different than conventional concrete. The addition of fibers enhanced the concrete's ability to carry stresses after cracking.

The reason for the advanced behaviour lies in the micro structure of the material. This advancement may lie in the size ratio of steel fiber and the maximum nominal size. Considering this size ratio is similar to the size ratio of steel reinforcement and maximum nominal aggregate size in ordinary reinforced, is a possible reason for the enhanced properties of UHPFRC. As a result UHPFRC is very similar to normal reinforced concrete but being reinforced at a micro level.

As a result UHPFRC possess the qualities to work in applications ranging from structural, architectural to artisan. Its use in structural application has been limited so far due to the lack of design codes available. The objective of this research was to investigate the adequacy of the current North American codes for the use of UHPFRC. Several mechanical properties design criteria were investigated. Parameters affecting various behaviours were also investigates and where applicable design equations were proposed.

[6.2]Mechanical Properties

[6.2.1] Fracture Energy

The results obtained from the fracture energy testing fortified the effect of fiber reinforcement. While normal and high strength concrete have fracture energy values of 110 N/m and 160 N/m, UHPFRC fracture energy testing yielded results that are approximately 10 times greater. In general UHPFRC didn't now follow the tensile behaviour of concrete, showing increase of carrying capacity after cracking as discussed in section [4.2].

While the fracture energy values are not used; the characteristic length, l_{ch}, is recommended for use in advanced design guidelines. The characteristic length has no physical meaning but is a representation of the ductility of a material. Results have shown that UHPFRC has a characteristic length of 731 mm; signifying a very ductile material.

[6.2.2] Tension Stiffening

The fiber reinforcement proved to have a distinct effect on the tensile strength and the cracking behaviour of concrete. When compared to ordinary concrete or high strength fiber reinforced concrete, UHPFRC has a more significant contribution in tension stiffening behaviour. Prior to cracking all types of concrete have a similar tension stiffening behaviour, however the post cracking characteristics proved to be rather dissimilar.

Typically, after cracking the contribution of concrete in tension is dramatically decreased. The introduction of fiber reinforcement tends to increase the post cracking tensile carrying capacity of concrete members. Results of this investigation have shown after cracking, due to the fiber reinforcement, UHPFRC maintained its tensile carrying capacity. In addition, test results have shown for concrete members under pure tension and having a reinforcement ratio under 2%; the steel reinforcement fails prior to the concrete member. Such behaviour is unprecedented for reinforced concrete members, due to the low tensile carrying capacity of concrete.

[6.2.3] Shear Friction

The present design equations do not provide accurate results for predicting the shear friction strength of UHPFRC. The test results provided in this research have correlated with the existing equation proposed by Khan and Mitchell (2002). To incorporate the effect of the fiber reinforcement the proposed Eq [4-6] proved to be accurate when compared to test results of concrete ranging from 30-160 MPa.

The proposed equation incorporates the effect of fiber reinforcement within the existing equation proposed by Khan and Mitchell (2002). The resultant equation predicts the shear friction strength of UHPFRC with an accuracy of 90%. The basis for the equation is including the effect of fibers on concrete is similar to the effect of steel reinforcement on concrete by crossing the cracks on the horizontal shear plane.

[6.3] Structural Behaviour

[6.3.1] Flexural Behaviour

All beams tested were design as shear critical beams, according to the CSA A23.3-04, however all beams failed in flexure. This is due to the lack of incorporating the fiber reinforcement within the current design equations. Both CSA A23.3 and ACI 318 proved to be rather conservative in predicting ultimate flexural capacity of UHPFRC beams. Typically, the concrete contribution in flexure is ignored in design codes after cracking. However, the test results have shown otherwise. Taking into consideration the results of the fracture energy and tension stiffening behaviour, it is clear that UHPFRC carries stresses after cracking. These observations can be directly applied to the behavior in flexure. Both proposed equations Eq. [5-2] and Eq. [5-3] have predicted the ultimate flexural capacity of UHPFRC with great accuracy. Eq. [5-2] incorporates the effect of the fiber reinforcement in terms of the modulus of rupture of the material. However, Eq. [5-3] incorporated the effect of fibers in terms of the fiber reinforcement's volume fraction.

The second proposed equation Eq. [5-3] predicted the ultimate flexural capacity of UHPFRC with 92% accuracy.

[6.3.2] Shear Behaviour

While none of the tested beams showed shear failure, multiple observations can be drawn from the test results. Yet again the current North American design codes proved to be inadequate in predicting the shear strength of UHPFRC. Also, the proposed equation from previous research proved to be inadequate for predicting shear strength of UHPFRC. It appears though the shear strength of UHPFRC is related to the tensile strength. The Japanese society for civil engineers recommendation for design of UHPFRC proved to be the most accurate for the shear capacity of the tested members.

Another speculation is incorporating the effect of fiber reinforcement, in terms of the fiber pull out strength. A method which related the shear strength of fiber reinforced concrete directly to the amount of fiber reinforcement crossing the shear failure plane.

[6.4] Recommendation for Future Work

The investigation carried out aimed to study the basic mechanical and structural behaviour of UHPFRC. Hence, a few limitations arise due to the lack of full depth investigation in one specific concept. As such much future work could be recommended based of the finding of this preliminary investigation. The following is a list of suggestion for future work:

[6.4.1] Fracture Energy:

The fracture energy test carried out in this research provided the basics for much greater concepts to be investigated. While the fracture energy is not directly used in the design of concrete structures, significant studies have been conducted to incorporate the fracture energy and behavior. Though it is not a representation of any physical property, l_{ch}, represents the brittleness of concrete. Numerous researches have gone into incorporating the characteristic length into design equation. For concrete beams without stirrups a model was developed by the Rilem Technical Committee represented (Hillerborg A. , 1985).

A later model was developed for shear strength of high strength concrete slabs represented by Eq [6-1] (Marzouk, Emam, & Hilal, 1998)

$$v_u = 0.88\, f_t \frac{c}{d}^{-0.4} \sqrt[3]{\rho \frac{l_{ch}}{h}} \qquad \text{[Eq.6-1]}$$

Where, *c* is the length of a side of a square column, *d* is the effective depth of slab, *h* is the total slab thickness, f_t is the uniaxial tensile strength of concrete and l_{ch} is the characteristic length

In design equation it is generally assumed that the shear strength is proportional to the tensile strength of concrete. However, many researchers argue, the use of the square root of the compressive strength to represent the tensile strength of concrete is not adequate when using HSC, HPC or UHPFRC. Hence, a major advantage is to incorporate the fracture energy within

[6.4.2] Tension Stiffening:

The tension stiffening behaviour results indicate the use of ordinary steel could prove rather obsolete due to the high tensile strength of UHPFRC. Thus, it is recommended to investigate the tension stiffening behaviour of UHPFRC reinforced with high strength steel. Also the use of other means of reinforcement such as Glass Fiber Reinforcing Polymer (GFRP) should be investigated.

[6.4.3] Shear Friction

The shear friction tests performed, provided a good starting point to an in-depth investigation. A recommendation for future work includes the shear friction behaviour of UHPFRC joint to other types of concrete. Also the joint surface and preparation should be investigated.

[6.4.4] Flexure and Shear Behaviour

The behaviour of UHPFRC beams under four point loading is by far the most essential portion of the investigation. For future studies the effect of fiber reinforcement should be studied. Investigating different fiber content and steel reinforcement should result in better understanding of the material's behaviour under flexure stresses.

The shear behaviour of concrete beams in general is a complicated matter. A full in depth investigation should be carried out to understand the material's behaviour. The many factors affecting shear strength (summarized in section **Error! Reference source not found.**) should be investigated; in specific, the concepts relating the shear strength to the fiber's pull out strength. Again the fiber content should be varied for a full understanding of the behaviour.

REFERENCES

Abrishami, H., & Mitchell, D. (1997). Influence of Steel Fibers on Tension Stiffening. *ACI Structural Journal* , 769-775.

ACI Committee 363 R. (2010). *Report on High-Strength Concrete.* Farmington Hills, USA.

Aoude, H., Belghiti, M., Cook, W., & Mitchell, D. (2012). Response of Steel Fiber-Reinforced Concrete Beams with and without Stirrups. *ACI* , 359-367.

Ashour, S., Hasanain, G., & Wafa, F. (1992). Shear Behavior of High-Strength Fiber Reinforced Concrete Beams. *ACI Structural Journal, V89, No 2* , 176-184.

Barr, B., Lydon , F., & Zhou, P. (1995). Fracture properties of high strength concrete with varyunf silica fumes content and aggregates. *Cement and Concrete Research* , 543-553.

Bunje, k., & Fehling, E. (2004). About shear force and punching shear resistance of structural elements of Ultra High Performance Concrete. *International Symposium on Ultra High Performance Concrete* (pp. 401-411). Kassel: structural Materials and Engineering Series.

Collins, M., & Kuchma, D. (1999). How Safe are our Large, Lightly Reinforced Concrete Beams, Slabs, and Footings? *ACI Structural Journal* , 482-191.

Concrete Committee, Japan Society of Civil Engineers. (2008). *Recommendation for Design and Construction of High Performance Fiber Reinforced Cement Composites with Multiple Fine Cracks (HPFRCC).* Japan Society of Civil Engineers.

Dawood, N., & Marzouk, H. (2012). Cracking and Tension Stiffening of High Strength Concrete Panels. *ACI STRUCTURAL JOURNAL* , 21-30.

Dibh, H., Oarra-Montesions, G., & Wight, J. (2011). Shear Stregnth MOdel For Fiber Reinforced Concrete Beams without Stirrup Reinforcement. *Journal of Structural Engineering* , 1039-1051.

Einsfeld, R., & Velasco, M. (2006). Fracture Prameters for High Preformence Concrete. *Cement and Concrete Research* , 576-583.

Elzanaty, A. (1986). Shear Capacity of Rienforced Concrete Beams Using High-Strength Concrete. *ACI Journal* , 290-296.

Emplemann, M. (2008). Improvemnt of the Post Fracture Behaviour of UHPC by Fibers. *Second International Symposium on Ultra High Preformance Concrete*, (pp. 177-184). Kassel, Germany.

Farny, J. A., & Panarese, W. *High-Strength Conrete.* Skokie, Illinois, USA: PCA.

Federal Highway Administration. (2006). *Material Property Characterization of Ultra-High Performance Concrete.* Georgetown: Research, Development, and Technology Turner-Fairbank Highway Research Center.

Fischer, G., & Li, V. (2002). Influence of Matrix Ductility on Tension-Stiffening Behavior of Steel Reinforced Engineered Cementitous Composites (ECC). *ACI Structural Journal* , 104-111.

Graybeal, B. (2008). Flexural behavior of an ultrahigh-Performance Concrete i-Girder. *Hournal of Bridge Engineering* , 602-610.

Hillerborg, A. (1985). *The Theoretical basis of a Method to Determine the Fracture Energy Gf of Concrete.* Lund: BORDAS-GAUTHIER-VILLARS.

Hillerborg, A. (1985). *The Theoretical Basis of a Method to Determine the Fracture Energy GF of Concrete.* Lund: BORDAS-GAUTHIER-VILLARS.

Hillerborg, A., Modeer, M., & Petersson, P. (1976). Analysis of crack formation and crack growth in concrete by means of fracture mechanics and finite elements . *Cement and Concrete Research* , 773-782.

Hilsdorf, H., & Brameshuber, W. (1991). Code-type formulation of fracture mechanics concepts for concrete. *International Journal of Fracture* , 61-72.

Hilsdorf, H., & Brameshuber, W. (1991). Code-type formulation of fracture mechanics concepts for concrete. *International Journal of Fracture* , 61-72.

Japan Concrete Institute Standard. (2003). *Method of test for fracture energy of concrete by used of notched beam JCI-S-001-2003.* Japan Concrete Institute Standard.

Khan , L., & Mitchell, A. (2002). Shear Friction Tests With High Strength Concrete. *ACI Structural Journal* , 98-103.

Kwak, Y., Eberhard, M., Kim , W.-S., & Kim, J. (2002). Shear Strength of steel Fiber-Reinforced concrete beams without Stirrups. *ACI Structural Journal* , 530-538.

Lafarge North America. (2011). Retrieved May 18, 2011, from Ductal: http://www.ductal-lafarge.com

Martin, J., & Stanton, J. (2007). Experimental Testing to Determine Concrete Fracture Energy Using Simple Laboratory Test Setup. *ACI Materials Journal* , 575-584.

Marzouk, H., & Chen, Z. (1995). Fracture Energy and Tension Properties of High Strength Concrete. *Materials in Civil Engineering* , 108-116.

Marzouk, H., Emam, M., & Hilal, M. (1998). Sensitivity of shear strength to fracture energy of high stregnth concrete slabs. *Canadian journel of civil Engineering* , 40-50.

Naraynan, R., & Darwish, I. (1987). Use of Steel Fibers as Shear Rienforcement. *ACI Structural Journal, V84, No3* , 216-227.

Petersson, P. (1980). Fracture Energy of Concrete: Method of Determination. *Cement and Concrete Research* , 79-89.

Rao, G., & Prasad, B. (2002). Fracture energy and softening behavior of high strength concrete. *Cement and Concrete Research* , 247-252.

Rao, G., & Prasad, B. (2002). Fracture energy and softening behaviour of high-strength concrete. *Cement and Concrete Research* , 247-252.

Rebentrost, m. (2008). Experience and Applicatios of Ultra high Performance concrete in Asia. *Second International Symposium on Ultra High Performance Concrete* (pp. 19-30). kassel, Germany: Structural Materials and Engineering Series.

Resplendino, J. (2004). First Recommendations for Ultra-High-Performance Concretes and Examples of Application. *International Symposium on Ultra High Performance Concrete* (pp. 79-89). Kassel, Germany: structural Materials and Engineering Series.

Rizk, E., Marzouk, H., Hussein, A., & Hossin, M. (2011). Effect of reinforcement ratio on punching capacity of RC plates. *Canadian Journal for Civil Engineering* , 729-740.

Roy, D., Gouda, G., & Bobrowsky, A. (1972). Very High Strength Cement Paste Prepared by Hot Pressing and Other High Pressure Techniques. *Concrete and Cement Research* , 349-366.

Sharma, A. (1986). Shear Strength of Fiber Reinforced Concrete Beams. *ACI Journal, Proceedings V.83, No 4* , 624-628.

Soranakom, C., & Mobasher, B. (2007). Closed-Form Solutions for Flecural Response of Fiber-Reinforced Concrete beams. *Journal of Engineering Mechanics* , 933-941.

Stramandinolie, R., & Rovere, H. (2008). An efficient tension-stiffening model for nonlinear analysis of reinforced concrete members. *Engineering Structures* , 2069-2080.

Wille, K., & Naaman, A. (2011). Ultra- High Performence Concrete and Fiber Reinforced Concrete: Achieving Strength and Ductility without Heat Curing. *Rilem* , 309-324.

Youdenfreund, M., Skalny, J., Mikhail, R., & Brunauer, S. (1972). Hardened Portland Cement Paste of Low porosity. *Cement and Concrete Research* , 331-348.

Zhou, F. (1995). Fracture Properties of High Strength Concrete with Varying Silica Fumes content and Aggregates . *Cement and Concrete Reseach* , 543-552.

Zhou, P., Barr, B., & Lydon, F. (1995). Fracture properties of high strength concrete with varying silica fume content and aggregates. *Cement and Concrete Research* , 543-552.